

**IMPROVEMENT OF POST-FAULT VOLTAGE RECOVERY  
PERFORMANCE UNDER HIGH RENEWABLE POWER  
PENETRATION IN A MICROGRID**

*by*

**Mohammad Saifullah Shawkat  
(0417062131)**

Submitted in partial fulfillment of the requirements of the degree of Master of Science in  
Electrical and Electronic Engineering



BANGLADESH UNIVERSITY OF ENGINEERING AND TECHNOLOGY  
DHAKA-1000, BANGLADESH  
August 2020

**IMPROVEMENT OF POST-FAULT VOLTAGE RECOVERY  
PERFORMANCE UNDER HIGH RENEWABLE POWER  
PENETRATION IN A MICROGRID**

*by*

**Mohammad Saifullah Shawkat  
(0417062131)**

Submitted in partial fulfillment of the requirements of the degree of Master of Science in  
Electrical and Electronic Engineering



Under the supervision of

**Dr. Nahid-Al-Masood**

Associate Professor

Department of Electrical and Electronic Engineering  
Bangladesh University of Engineering and Technology (BUET)

BANGLADESH UNIVERSITY OF ENGINEERING AND TECHNOLOGY

DHAKA-1000, BANGLADESH

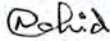
August 2020



## CERTIFICATION OF THESIS

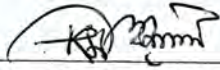
The thesis titled “**IMPROVEMENT OF POST-FAULT VOLTAGE RECOVERY PERFORMANCE UNDER HIGH RENEWABLE POWER PENETRATION IN A MICROGRID**” submitted by **Mohammad Saifullah Shawkat**, Student ID: 0417062131, Session: April/2017 has been accepted as satisfactory in partial fulfillment of the requirement for the degree of Master of Science (M.Sc.) in Electrical and Electronic Engineering on 25 August,2020.

### BOARD OF EXAMINERS



Dr. Nahid-Al-Masood  
Associate Professor  
Department of Electrical and Electronic Engineering  
Bangladesh University of Engineering and Technology, Dhaka, Bangladesh

Chairman  
(Supervisor)



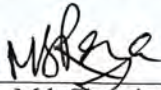
Dr. Md. Kamrul Hasan  
Professor & Head  
Department of Electrical and Electronic Engineering,  
Bangladesh University of Engineering and Technology, Dhaka, Bangladesh

Member  
(Ex- officio)



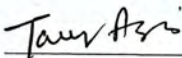
Dr. Mohammad Jahangir Alam  
Professor  
Department of Electrical and Electronic Engineering  
Bangladesh University of Engineering and Technology, Dhaka, Bangladesh

Member



Dr. Md. Shamim Reza  
Professor  
Department of Electrical and Electronic Engineering  
Bangladesh University of Engineering and Technology, Dhaka, Bangladesh

Member



Dr. Tareq Aziz  
Professor  
Department of Electrical and Electronic Engineering  
Ahsanullah University of Science and Technology, Dhaka, Bangladesh

Member  
(External)

## **CANDIDATE'S DECLARATION**

I, Mohammad Saifullah Shawkat, declare that this thesis titled, "IMPROVEMENT OF POST-FAULT VOLTAGE RECOVERY PERFORMANCE UNDER HIGH RENEWABLE POWER PENETRATION IN A MICROGRID" and the work presented in it are fully my own in partial fulfillment of the requirement for the degree of Master of Science (M.Sc.) in Electrical and Electronic Engineering. I confirm that no part of this thesis has been submitted anywhere else. Others' works that have been quoted are clearly attributed with source.



---

Mohammad Saifullah Shawkat

*Dedicated to my parents...*

## Table of Contents

List of Figures.....	viii
List of Tables .....	xi
Abbreviations.....	xii
Nomenclature.....	xiii
Acknowledgement .....	xiv
Abstract.....	xv
CHAPTER 1 Introduction.....	1
1.1 Introduction.....	1
1.1.1 Background.....	1
1.1.2 Microgrid .....	2
1.1.3 Islanded Mode Operation of a Microgrid .....	4
1.1.4 SVC as Reactive Power Compensator.....	6
1.2 Objectives of the Present Thesis .....	7
1.2.1 Thesis Layout.....	8
CHAPTER 2 Literature Review .....	9
2.1 Voltage and Frequency Control in Microgrids .....	9
2.2 Energy Management in Microgrids.....	11
2.3 SVC for System Stability.....	12
2.4 Load Modeling .....	13
2.5 Research Gaps and Motivation .....	13
CHAPTER 3 Grid Code and Proposed Methodology .....	15
3.1 Grid Code for Microgrid Operation .....	15
3.2 Proposed Methodology .....	16
3.2.1 Load Flow Calculation.....	16
3.2.2 Reactive Power Margin.....	19

3.2.3	Load Modeling.....	20
3.2.4	Steps of the SVC Placement Algorithm.....	20
CHAPTER 4 Results and Discussions.....		22
4.1	Introduction .....	23
4.2	Test System and Simulation Tool .....	23
4.3	Calculation of Reactive Power Margin .....	25
4.4	Simulation Scenarios.....	25
4.5	Simulation Results and Analyses .....	26
4.5.1	Case-1: 23% RE Penetration.....	26
4.5.2	Case-2: 30% RE Penetration.....	33
4.5.3	Case-3: 40% RE Penetration.....	41
4.5.4	Case-4: 45% RE Penetration.....	43
4.5.5	Case-5: 50% RE Penetration.....	45
4.6	Validation of the Proposed Methodology .....	48
4.7	Effect of Load Modeling .....	51
4.7.1	Constant Current Type Load Model .....	52
4.7.2	Constant Power Type Load Model .....	53
CHAPTER 5 Conclusions.....		54
5.1	Conclusions .....	55
5.2	Future Research Scopes .....	56
Bibliography .....		56



# List of Figures

Figure 1.1: Carbon emission due to electricity production. [1] .....	1
Figure 1.2: Schematic diagram of a microgrid [9].....	4
Figure 1.3: Schematic diagram of a SVC .....	7
Figure 3.1: Flowchart of load flow calculation.....	18
Figure 3.2: Reactive power margin [68].....	19
Figure 3.3: Flow chart of the proposed SVC placement algorithm .....	22
Figure 4.1: Single line diagram of the test microgrid [42].....	24
Figure 4.2: Voltage at PCC1 (Bus 4) at 23% RE penetration.....	27
Figure 4.3: Power output from DER1 at 23% RE penetration.....	27
Figure 4.4: Voltage at PCC4 (Bus 41) at 23% RE penetration.....	28
Figure 4.5: Power output from DER4 at 23% RE penetration.....	28
Figure 4.6: Voltage at PCC3 (Bus 50) at 23% RE penetration.....	29
Figure 4.7: Power output from DER3 at 23% RE penetration.....	29
Figure 4.8: Voltage at PCC2 (Bus 100) at 23% RE penetration.....	30
Figure 4.9: Power output from DER2 at 23% RE penetration.....	30
Figure 4.10: Motor speed at bus 37 (indication of blackout) at 23% RE penetration.....	31
Figure 4.11: Voltage at PCC1 (Bus 4) at 23% RE penetration with SVC .....	31
Figure 4.12: Voltage at PCC2 (Bus 100) at 23% RE penetration with SVC .....	32
Figure 4.13: Voltage at PCC3 (Bus 50) at 23% RE penetration with SVC .....	32
Figure 4.14: Voltage at PCC4 (Bus 41) at 23% RE penetration with SVC .....	33
Figure 4.15: Voltage at PCC1 (Bus 4) at 30% RE penetration.....	34
Figure 4.16: Power output from DER1 at 30% RE penetration.....	34
Figure 4.17: Voltage at PCC4 (Bus 41) at 30% RE penetration.....	35
Figure 4.18: Power output from DER4 at 30% RE penetration.....	35
Figure 4.19: Voltage at PCC3 (Bus 50) at 30% RE penetration.....	36
Figure 4.20: Power output from DER3 at 30% RE penetration.....	36
Figure 4.21: Voltage at PCC2 (Bus 100) at 30% RE penetration.....	37
Figure 4.22: Power output from DER2 at 30% RE penetration.....	37
Figure 4.23: Motor speed at bus 37 (indication of blackout) at 30% RE penetration.....	38
Figure 4.24: Voltage at PCC1 (Bus 4) at 30% RE penetration with SVC .....	39
Figure 4.25: Voltage at PCC2 (Bus 100) at 30% RE penetration with SVC .....	39
Figure 4.26: Voltage at PCC3 (Bus 50) at 30% RE penetration with SVC .....	40
Figure 4.27: Voltage at PCC4 (Bus 41) at 30% RE penetration with SVC .....	40
Figure 4.28: Voltage at PCC1 (Bus 4) at 40% RE penetration.....	41
Figure 4.29: Voltage at PCC4 (Bus 41) at 40% RE penetration.....	42
Figure 4.30: Voltage at PCC1 (Bus 4) at 40% RE penetration with SVC .....	43
Figure 4.31: Voltage at PCC1 (Bus 4) at 45% RE penetration.....	44
Figure 4.32: Voltage at PCC1 (Bus 4) at 45% RE penetration with SVC .....	45

Figure 4.33: Voltage at PCC1 (Bus 4) at 50% RE penetration.....	46
Figure 4.34: Voltage at PCC1 (Bus 4) at 50% RE penetration with SVC.....	47

# List of Tables

Table 3.1: Voltage recovery time under various scenarios [67] .....	15
Table 4.1: Types and location of DER units.....	24
Table 4.2: Reactive power margin of five most vulnerable buses .....	25
Table 4.3: Simulation cases .....	25
Table 4.4: Post-fault voltage with SVC after 2s of fault occurrence at 23% RE penetration .....	33
Table 4.5: Post-fault voltage with SVC after 2s of fault occurrence at 30% RE penetration .....	41
Table 4.6: Post-fault voltage after 2s of fault occurrence at 40% RE penetration .....	42
Table 4.7: Post-fault voltage with SVC after 2s of fault occurrence at 40% RE penetration .....	43
Table 4.8: Post-fault voltage after 2s of fault occurrence at 45% RE penetration .....	44
Table 4.9: Post-fault voltage with SVC after 2s of fault occurrence at 45% RE penetration .....	45
Table 4.10: Post-fault voltage after 2s of fault occurrence at 50% RE penetration .....	46
Table 4.11: Post-fault voltage with SVCs after 2s of fault occurrence at 50% RE penetration.....	47
Table 4.12: Post-fault voltage with exiting approach at 23% RE penetration .....	48
Table 4.13: Post-fault voltage with exiting approach at 30% RE penetration .....	49
Table 4.14: Post-fault voltage with exiting approach at 40% RE penetration .....	49
Table 4.15: Post-fault voltage with exiting approach at 45% RE penetration .....	50
Table 4.16: Post-fault voltage with exiting approach at 50% RE penetration .....	50
Table 4.17: Performance comparison under various RE penetration .....	51
Table 4.18: Post-fault voltage for constant current load at 23% RE penetration.....	52
Table 4.19: Post-fault voltage for constant current load at 30%, 40%, 45% and 50% RE penetration .....	52
Table 4.20: Post-fault voltage for constant power load at different RE penetration.....	53
Table 4.21: Comparison of SVC rating for different load models.....	53

# Abbreviations

AVI	Adaptive Virtual Impedance
BESS	Battery Energy Storage Systems
CI	Connection Interface
DAC	Difference Angle Compensator
DER	Distribute Energy Resource
DG	Diesel Generator
DR	Demand Response
DSM	Demand Side Management
EMS	Energy Management System
ENN	Elman Neural Network
FACTS	Flexible AC Transmission System
FESS	Flywheel Energy Storage System
FLC	Fuzzy Logic Controller
FRL	Frequency Restoration Loop
HESS	Hybrid Energy Storage System
LC	Load Control
MC	Microsource Control
MGCC	Microgrid Central Management System
MSC	Mechanically Switched Capacitors
PCC	Point of Common Coupling
PI	Proportional Integral
PV	Photovoltaic
RE	Renewable Energy
SOFC	Solid Oxide Fuel Cell
SVC	Static VAR Compensator
TCL	Thermostatically Controlled Loads
TCR	Thyristor Controlled Reactor
TSC	Thyristor Switched Capacitor
WT	Wind Turbine

# Nomenclature

$S$	Apparent Power
$P$	Real Power
$Q$	Complex Power
$I$	Current
$\theta$	Angle
$V$	Voltage

# Acknowledgement

It takes a lot to complete an M.Sc. thesis. I would like to take this moment to thank the Almighty to provide me with the opportunity to complete my thesis work. Without his kind mercy, it would not have been possible for me to carry out this work in healthy physical condition.

I would like to express my heartiest gratitude to my supervisor, Dr. Nahid-Al-Masood, Associate Professor, Department of Electrical and Electronic Engineering, Bangladesh University of Engineering and Technology (BUET), Dhaka, for his kind supervision of this work. He was always there with his guidance for me whenever I needed any. Without his help, it would not have been possible for me to go through with my works. I would like to express my gratefulness to him for his patience and humbleness throughout this thesis and the way he advised me to take the right decisions at the right time.

Last but not the least, I would like to thank my parents, my brother and sisters, my friends and my all well-wishers for the support they have provided me with throughout this difficult time.

# Abstract

Blackouts, although rare, are considered as catastrophic incidents in power systems which can adversely affect day-to-day life. To combat this disastrous event, among many others, microgrids have emerged as a potential solution. This is mainly due to the capability of a microgrid to operate in an islanded mode after a large disturbance in the main grid, if necessary. However, even in an islanded microgrid, unacceptable voltage recovery performance after a fault may cause the cascading tripping of distributed generators (also known as Distributed Energy Resources – DERs). This may subsequently result in a blackout in a microgrid in extreme case. To enhance voltage control capability in microgrids, a number of research works are reported in the literature. However, these methods lack the capability of improving the post-fault voltage recovery performance at the Point of Common Coupling (PCC) of DERs in an islanded microgrid, especially under high renewable power penetration. Therefore, further investigations are still required to address this important research gap. To this end, Static VAR Compensator (SVC), which provides reactive power support, can be a worthwhile choice.

In the above aspect, a methodology for the placement of SVC to improve the post-fault voltage recovery performance at the PCC of DERs under substantial renewable power penetration in a microgrid is proposed in this thesis. Also, the impact of load model parameters on the voltage recovery performance at the PCC of DERs following a severe fault in a microgrid is explored. The proposed methodology is applied to a test microgrid network under various renewable power penetration scenarios. The effectiveness of the developed technique is validated by comparing its performance with that an existing method.

The findings of this research work provide significant insight into the capability of the SVC to improve post-fault voltage recovery performance in an islanded microgrid with high renewable power penetration. Eventually, the developed approach mitigates the risk of cascading tripping of DERs and subsequent blackout to ensure resilient operation of a microgrid.

# CHAPTER 1

## Introduction

### 1.1 Introduction

#### 1.1.1 Background

For decades, centralized power plants were the traditional way of delivering electricity from the point of production to customers. The traditional energy sources are all primarily non-renewable energy sources. Its extensive use has led to the rapid depletion of their reserves. In addition, the pollution caused by the non-renewable energy sources is having a huge negative impact on the environment. During the time of construction and generation, traditional power plants have environmental impacts like air pollution, water pollution, land pollution and etc. From the Figure 1.1 below, the severity of the carbon emission caused by electricity production can be observed for various years. Note that it was around round 33 gigatonnes during 2019. However, the positive side is that it has flattened up due to increase in electricity generation from renewable sources.

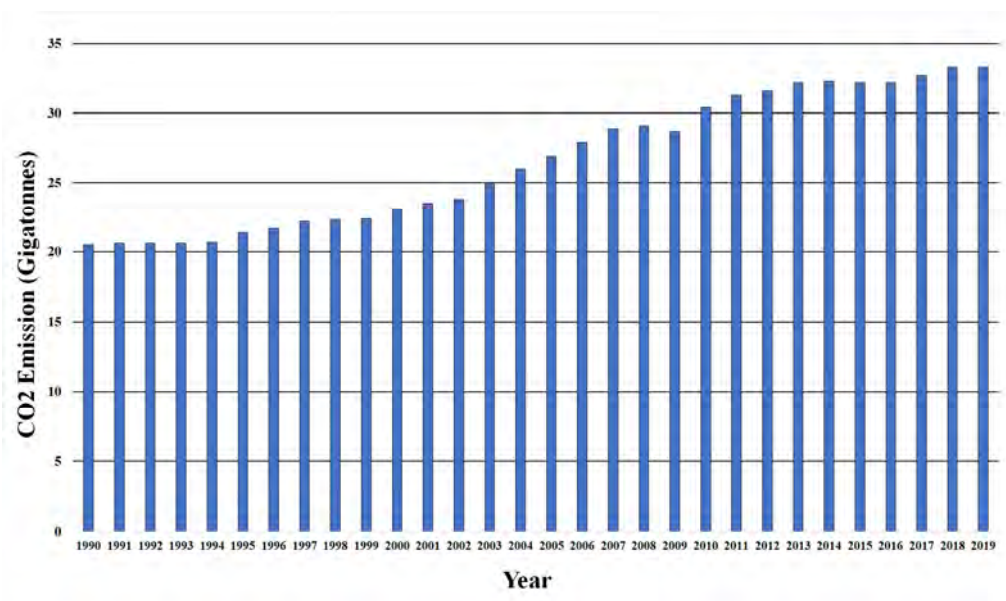


Figure 1.1: Carbon emission due to electricity production. [1]



Addressing the global demand for electricity from renewable energy sources is one of the challenging tasks due to a number of technical and legislative issues. Clean energy systems are needed to meet the increasing global demand for electricity, with decreased reliance on fossil fuel and related environmental harm. Renewable energy sources have the potential to meet this growing demand for electricity, since they are regarded as cleaner alternatives for fossil fuels.

In conventional power system, electricity is supplied from large power plants, mostly centralized, covering large areas. Along with the environmental impact, one of the main problems in the conventional power system is that when any type of problem occurs (e.g. electrical fault, line tripping, generator outages etc.), a blackout may be incurred in the whole grid or in a large portion of the grid. For instance, in November 1, 2014, 160 million Bangladeshis faced a blackout for about 10 hours when the 400 kV transmission line was tripped at a sub-station in Bheramara in Kushtia which was bringing around 450 MW of power from India [2].

In addition, in the centralized power grid, there are some disadvantages like high costs, operating challenges, meeting safety and reliability standards etc. In recent times, the pressure on the transmission network is rising at an unprecedented rate due to increased power demand. Also, there are areas that are too remote to be connected to the main grid. Even if it is done, the transmission cost and complexity of transmission become extensively high, which result in very high cost for electricity.

Therefore, there is a need for small grids relying on renewable energy-based power network to mitigate environmental problems and risk of blackouts. To this end, microgrids can be a worthwhile solution [3].

### **1.1.2 Microgrid**

A microgrid can be described as an independent power network using local distributed energy resources (DERs) to supply grid backup or off-grid power to meet local electricity needs or to be connected to the main grid to enhance the capacity of the main grid [4]. It is an effective way to integrate the advantages of distributed generation and to provide a modern technical way of implementing grid-connected renewable energy sources on a wide scale [5]. It is a network of small distributed energy recourses (DERs) operated as a collective unit to cater the local demand when it is isolated from the main grid [6].

In many ways, microgrids have some similarities with the traditional power grids. They consist of power generation, distribution, and controls such as voltage regulation and switch gears like traditional grids. However, microgrids differ from conventional electrical grids by providing closer proximity between power generation and power consumption. It results in improved efficiency and decreased transmission loss. Also, microgrids provide power quality, reliability and security for end users and operators in a cost competitive and efficient manner which eventually enables smart grid technology integration [7]. Furthermore, one of the main features of microgrids is their ability to operate in islanded mode (i.e. disconnected from the main grid) when needed [8].

### **1.1.2.1 Microgrid Structure**

The generalized structure and topology of a microgrid is shown in the Figure 1.2 [9]. The choice and the combination of possible elements determines the capability of a microgrid. Solid-state switches and even back-to-back (AC / DC / AC) power electronic inverters can be used as the connection interface to the utility network electro-mechanical circuit breaker. To balance the power flow, some kind of rapid-working energy consumption and injection capacity is usually required, which can also be any energy storage system. The load characteristics and DERs determine the need for storage of energy and power quality. For extra control and speed, additional power electronics interface to the units can be used. Some degree of central control is required for the grid to operate as a system. Common microgrid state variables, instantaneous phase voltages and currents at the point of coupling must be regulated. The required communication may be done through telecommunication line, a signal superimposed on the network voltage (power line carrier) or even by modulation of the frequency.

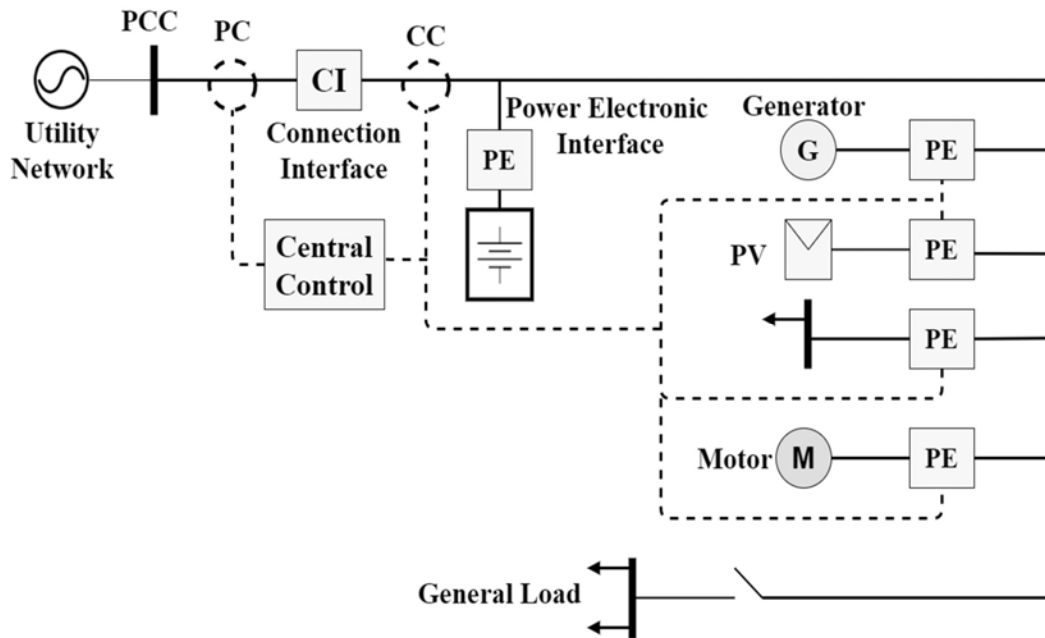


Figure 1.2: Schematic diagram of a microgrid [9]

The operating principle of a microgrid is heavily dependent on its operating strategies. Commonly, there are two modes of operation: one is grid connected operation and the other one is islanded mode operation. Therefore, it has two transient states that correspond to the transitions between the two modes. During all these conditions, it must remain stable and meet the grid code.

### 1.1.3 Islanded Mode Operation of a Microgrid

As a microgrid has its own power generation units, which are adequate to support the connected loads, it can function in islanded mode [10]. The ultimate goal of microgrids in islanded mode is to allow the network to function even in adverse circumstances such as main grid disruptions, high main grid power prices etc. But in islanded mode of operation, microgrid must supply priority loads first such as hospitals, transportation and telecommunications by utilizing the DERs. However, islanded mode operation requires more maintenance and technical expertise due its higher risk of outage because of limited generation. There must be

an energy management system (EMS) [11] to handle power resources to ensure the availability of top priority grid-connected customers and to ensure enough power supply to other connected loads. The consistency of power supply in islanded mode depends on installed DER capacity, proper energy management and other grid dynamic behavior related to voltage and frequency.

### **1.1.3.1 Operating Principle in Islanded Mode**

Opening the upstream switches at the interconnecting substation in the time of any emergency initiates islanding process of a microgrid [12]. Microgrid central management system (MGCC) [13] must perform some functions immediately, such as [10]:

- To restore voltage and frequency
- To determine connection and disconnection's policies of loads
- To optimize the operation based on prices of energy market, weather conditions and load profile
- To manage the buying and selling of power
- To guarantee a smooth reconnection and islanding process

MGCC interacts with local controllers such as Load Control (LC) and Microsource Control (MC) to ensure seamless operation [14]. MCs control the active and reactive power generations of each microsource and LCs prioritize the types of load. This approach follows a hierarchy based on ANSI/ISA-95, an international standard for developing an automated interface between enterprise and control systems. This is adapted for microgrid in three control step which is primary control, secondary control and tertiary control. The primary control uses the droop method to emulate the synchronous machines behavior. Secondary control ensures the voltage and frequency restoration by changing the operating points to synchronize the microgrid with the utility. The tertiary control is only used in connected mode to control the power flow between the grid and utility.

### **1.1.3.2 Voltage Instability in Microgrid**

Cascading failure [15] is a term that is basically associated with power system networks and transmission line. However, a micorgrid operating in islanded mode may be prone to cascaded failure of the DER units due to its limited supply source and inadequate post disturbance voltage recovery performance when any fault occurs in the system.

In an islanded microgrid, cascading contingency is instigated by any initial disturbance like faults in transmission lines or buses, failure of protection devices, improper operational settings of the equipment, damaged components due to various reasons. Furthermore, the increase share of the DERs, failure of control and protection mechanisms may lead to subsequent tripping of the DER units. Such events consequently may lead to a complete blackout of the whole microgrid [16].

With the increase of renewable power penetration in a microgrid, the post fault voltage recovery performance becomes even more complex. For instance, a small island system of Crete in Greece faced such type of problem due to fault originated voltage dips when 33 DER tripping events occurred in a period of 3 years [17]. In the same way, wind turbines tripping that were acting as DER units played a significant role in the development of the catastrophic European blackout in 2006 [18].

### **1.1.4 SVC as Reactive Power Compensator**

Static VAR Compensator (SVC) is a power electronic device for providing fast-acting reactive power on high-voltage electricity transmission networks. SVCs are basically Flexible AC Transmission System (FACTS) devices that have the capability to regulate voltage and stabilize the system [19]. If the reactive load is capacitive (leading), the SVC will use thyristor controlled reactors (TCRs) to consume VAR from the system. Under inductive (lagging) conditions, the capacitor banks are automatically switched on to supply VAR. This is how appropriate voltage control can be achieved using a SVC.

Figure 1.3 shows the overview of a SVC. The static VAR compensator system is basically a combination of a shunt capacitor bank and a thyristor controlled shunt reactor. The capacitors in the bank can be switched on and off individually. The capacitors can be switched with thyristors (TSC) or can be permanently (mechanically) connected (MSC).

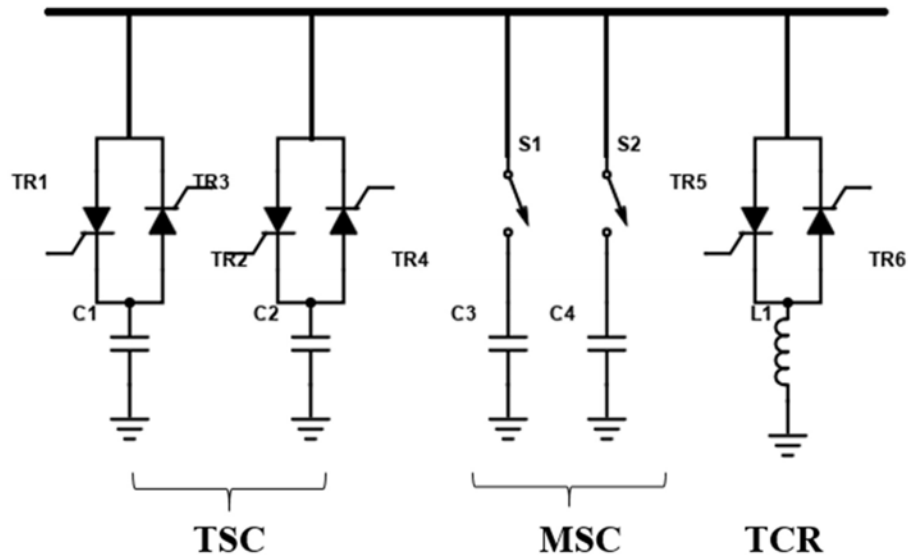


Figure 1.3: Schematic diagram of a SVC

## 1.2 Objectives of the Present Thesis

It is evident that unacceptable post-fault voltage recovery (which is effectively an indication of voltage stability) in an islanded microgrid may cause cascading tripping of DERs and a subsequent blackout. To overcome this challenge, SVCs can play a significant role by enhancing the post-fault voltage recovery at the points of common coupling (PCCs) of DERs in a microgrid. The instantaneous reactive power support from SVC after a fault can help the voltages at PCCs to improve over acceptable limits within desired time frame.

The specific objectives of the present study are:

1. To develop a methodology for the placement of SVC to improve the post-fault voltage recovery performance at the PCC of DERs under substantial renewable power penetration in a microgrid.
2. To analyze the impact of load model parameters on the voltage recovery performance at the PCC of DERs following a severe fault in a microgrid.
3. To investigate the effectiveness of the proposed methodology in a test microgrid network under various renewable power penetration scenarios.

The possible outcome of this thesis will be a new methodology for placing SVC to enhance post-fault voltage recovery performance during high renewable power penetration in a microgrid. The developed approach will mitigate the risk of cascading tripping of DERs and subsequent blackout to ensure resilient operation of a microgrid

### **1.2.1 Thesis Layout**

The thesis consists of five chapters. Following the introduction in Chapter 1, a comprehensive literature review is performed in Chapter 2 to identify the motivation and research gap. Afterwards, grid codes and proposed methodology are presented in detail in Chapter 3. Later on, simulation results and analyses are inclusively provided in Chapter 4. Finally, the key findings are summarized followed by future research scopes in Chapter 5.

## CHAPTER 2

# Literature Review

By 2050, the global demand for energy is predicted to be more than double of the present demand [1]. As such, dependence from fossil fuel has to be shifted towards renewable energy sources. Therefore, renewable energy based microgrid emerges as a profound solution. But in an islanded microgrid with a high renewable energy (RE) penetration, the voltage instability problem may become a severe issue. In particular, unacceptable voltage recovery at the PCCs of DERs after any disturbance can even lead to a complete blackout of the whole microgrid. Use of SVC has been a reliable source to improve voltage stability mainly in the large grids, which can also be considered as one of the most attractive choices to overcome voltage instability in microgrids. A comprehensive review on the most relevant studies and the recent works on microgrids, SVC and load modeling are presented in this chapter. Also, from the literature review, research gaps are identified.

### 2.1 Voltage and Frequency Control in Microgrids

To enhance voltage control capability in microgrids, a number of research works have been performed over the years. These include optimization in the placement and the size of the distributed energy sources, proper management of the energy storage devices and their control strategies.

Dehkordi 2017 [20], based on backstepping control and a high order sliding mode differentiator, presented a nonlinear control strategy for voltage in an islanded microgrid. The authors proposed a controller, which robustly regulates the voltages in a microgrid. Also, parametric uncertainties, load imbalances and nonlinear loads with harmonic currents were taken into consideration. Hirase 2018 [21] showed how voltage and frequency deviation can influence the stability of a microgrid using algebraic-type virtual synchronous generator (VSG) with a minimal number of parameters through simulations. Siddique 2019 [22] proposed a control system for voltage and frequency under dynamic system conditions in an islanded microgrid using a robust modified adaptive proportional integral derivative (PID) controller. Kim 2011 [23] presented a cooperative control strategy for the components of the microgrid



working in islanded mode using a pilot plant to maintain desired voltage level at the PCC of the DERs.

One of the most widely used strategies to control the voltage and frequency in a microgrid is the use of energy storage devices, battery energy storage systems (BESS) in particular. In recent times, for microgrids with high RE penetration, Garmabdari 2020 [24] proposed an effective solution to combat with the voltage fluctuations of the DERs using BESS. The authors developed a multi-objective mixed-integer quadratic model to construct a BESS capacity optimization algorithm. In addition, a novel coordination strategy among thermostatically controlled loads (TCLs), photovoltaic (PV) power systems, BESS and a diesel generator with demand side management (DSM) was presented by Acharya 2017 [25] for islanded microgrids. The control strategy that they used ensures IEEE Standard 1547 and at the same time maintains quality of service (QoS). A similar frequency control scheme was proposed by Serban 2014 [26] where they used BESS active power response governed by a frequency controller with two layers. It combines a conventional droop control with a virtual inertia function to improve system stability. Vigneys 2016 [27] used solid oxide fuel cell (SOFC) along with BESS to control the voltage and frequency in an islanded microgrid based on fuzzy logic controller (FLC) where SOFC was used as a backup generator. They showed the effectiveness of FLC over the conventional proportional integral (PI) controller in their work.

In addition to the above, a number of researchers have focused on the optimal siting and sizing of the energy storage devices and their control mechanism. García-Plaza 2018 [28] proposed a new peak shaving algorithm, which tracks the peak output of a BESS to avoid reverse power flow in case of the output power being too high. Fortenbacher 2017 [29] proposed a model predictive control (MPC) based strategy for BESS control while Palizban 2015 [30] proposed a decentralized control method for State of Charge (SoC) based on a modified droop control. [31-36] shows different strategies for the optimal sizing and siting of the energy storage devices which includes DC power flow approximation [31], Grey Wolf Optimization [32], Particle Swarm Optimization (PSO) [33], PSO incorporating demand response [34], optimal charging of the battery units [35] and multi-objective PSO [36]. Alternative energy storage devices have also been proposed in [37-39] instead of BESS to enhance the voltage and frequency control for islanded microgrids. These include Battery-supercapacitor Hybrid Energy Storage System (BSHS) [37], Flywheel Energy Storage System (FESS) [38], Air Source Heat Pump (ASHP) in a Photovoltaic/Battery Energy Storage System (PV/BESS) [39].

Voltage restoration in a microgrid has always been a challenge. For inverter based islanded microgrid, Pilloni 2017 [40] designed an ad-hoc chattering-free second-order sliding-mode controller for voltage restoration of the DERs. Soto 2012 [41] used a novel time-domain technique for single phase loads for voltage restoration of the DERs. Also, Aziz 2019 [42] used BESS to improve voltage stability in an islanded microgrid.

## 2.2 Energy Management in Microgrids

Due to its diverse and distributed energy resources, energy management in microgrids has been a challenging task. Several researchers have focused on this issue to find a comprehensive management system for the energy resources in a microgrid. For instance, Karavas 2015 [43] proposed a decentralized energy management system for an islanded polygeneration microgrid to provide an independent control scheme for each unit of the system. It avoids malfunction of rest of the units when any disturbance occurs in any of the units using a multi agent based Fuzzy Cognitive maps. The authors also showed comparative analysis between the proposed methodology and the conventional centralized control strategy. Besides, for autonomous polygeneration microgrids, another control strategy was developed by Kyriakarakos 2012 [44] that uses petri nets (PN) alongside fuzzy cognitive maps (FCMs). Here, the PN works as an activator for FCMs. For dynamic energy management of microgrids, a hetero-functional graph theory based strategy was suggested by Schoonenberg 2017 [45]. In the same year, Anvari-Moghaddam 2017 [46] proposed a multi agent based energy management system (EMS) to design an optimized control of an islanded microgrid with high RE penetration. In their work, the different agents cooperate with each other to gain a suitable optimum operating principle for the integrated energy system (IES).

A control strategy for Microgrid Supervisory Controllers (MGSC) and EMS was established by Meng 2016 [47]. In addition, Chettibi 2018 [48] used an online-trained Elman Neural Network (ENN) based controller for grid connected microgrids while Sedighizadeh 2019 [49] used a combination of Differential Evolutionary (DE) and Modified PSO (MPSO) algorithms considering to minimize the operation cost and emission in an islanded microgrid. To protect microgrid against load shedding, a power management scheme was proposed by Koochi-Kamali 2016 [50] to prevent the under frequency load shedding (UFLS) using BESS to compensate for the power mismatch in an islanded microgrid. They developed a methodology to find out the rate of change of frequency for efficient power output using a two outer loop

controls. These are frequency restoration loop (FRL) and difference angle compensator (DAC) loop. These loops ensure smooth transition between grid connected mode and islanded mode of operation.

Very recently, Nasr 2020 [51] proposed a new energy management system that considers the voltage instability and generation contingency constraints in an islanded microgrid. In their paper, based on a coordination of unit commitment-optimal power flow (UC-OPF), they introduced a multi-objective security constrained microgrid energy management system (MOSC-MEMS). Moreover, a dispatch algorithm was proposed by Wang 2018 [52] for microgrid EMS in order to improve performance in seven operating conditions. These include two steady state operating mode (grid connected and islanded), four transition mode (preparing for disconnection, transitioning to islanding, preparing for reconnection and transitioning to grid-connected) and one emergency operating mode (back-start operation). Also, Harmouch 2018 [53] implemented a decentralized multiagent EMS (DMA-EMS) to manage a cluster of microgrids.

## 2.3 SVC for System Stability

SVC (also known as Static VAR System – SVS) has long been considered as a reliable source to provide fast-acting reactive power for the stabilization of the system voltage, especially for conventional grids. Kincic 2005 [53] presented the advantage of the SVC for load centers in achieving a regulated voltage control for a system having large number of DERs. Chen 1996 [54] proposed an algorithm for Fixed Capacitor Thyristor Controlled Reactor (FC-TCR) type of SVC to balance a system dynamically with individual phase control scheme for each SVC. They also showed that SVC can help to improve the power factor of the system. Cathey 2002 [55] proposed a novel control scheme for the SVC to enhance transient stability of a large-scale power system.

Application of SVC in microgrids is a fairly new concept. Gabbar 2014 [56] developed a high-performance dynamic model for a microgrid consisting DERs and BESS. In their work, they showed that a microgrid with SVC can achieve the grid code requirements like bus voltages stabilization, reduction of feeder losses, power factor enhancement and mitigation of total harmonic distortion. Further, Mohanty 2015 [57] gave the idea of application of ANN based SVC controller for voltage stability in an islanded microgrid. Lately, Viswavandya 2019 [58] presented an algorithm to gain optimum voltage control in islanded microgrids using SVC.

However, the advantage of SVC in improving the post-fault voltage recovery performance of an islanded mode microgrid with high RE penetration is still needed to be investigated properly.

## 2.4 Load Modeling

The voltage stability of a power system considerably depends on the type of loads connected to the buses. For a system consisting different types of static and dynamic loads, the loads need to be accurately modeled to achieve stability of the grid following a disturbance. Renmu 2006 [59] developed a measurement-based composite load model using multi-curve identification technique. Also, the identification of nature of load was presented by Arif 2017 [60] while Mota 2004 [61] presented a load modeling approach using dynamic load parameters estimation. A robust time-varying load modeling technique using recursive least square (RLS) to estimate the ZIP (impedance-current-power) parameters was proposed by Zhao 2016 [62]. A new idea for modeling dynamic loads using the data from billing information was developed by Vaahedi 1988 [63].

Furthermore, the impact of load modeling for a wind energy-based system was presented by El-Shimy 2018 [64]. Singh 2016 [65] presented the effect of distributed generation placement with different load models and SVC using genetic algorithm. In recent years, Hashemi-Dezaki 2019 [66] developed a methodology to quantify the load model parameters in a smart grid environment.

## 2.5 Research Gaps and Motivation

Based on the above discussion, a considerable number of studies have focused on the voltage and frequency control and energy management of microgrids. However, these methods lack the capability of improving the post-fault voltage recovery performance at the PCC of DERs in an isolated microgrid, especially under high renewable power penetration. Therefore, further investigations are still required to address this important issue. Also, in an islanded microgrid under high renewable penetration, the impact of load modeling on the post-fault voltage recovery performance is yet to be explored.

To address the above research gaps, this thesis proposes a technique for SVC placement in an islanded microgrid for enhancing the post-fault voltage recovery response to avert the cascading tripping of DERs. Also, the effect of load modeling on the voltage recovery performance is comprehensively analyzed in this thesis.

## CHAPTER 3

### Grid Code and Proposed Methodology

In this chapter, at first, the grid code of microgrid operation is presented. Then the proposed methodology to improve the post-fault voltage recovery performance in an islanded microgrid is explained in detail.

#### 3.1 Grid Code for Microgrid Operation

Different standards are available for the design, operation and integration of microgrids. Over the years, IEEE Standard 1547-2018 [67] is widely accepted to set rules for guiding microgrid operation. Table 3.1 shows the recommended voltage recovery time at the PCC of DER under various voltage excursion cases. Here, the voltage recovery time refers to the time required for the PCC voltage to get back to a given value after the occurrence of a fault. If the PCC voltage fails to reach a value less than an under-voltage threshold or greater than an over-voltage threshold within respective recovery time, the corresponding DER will trip.

Table 3.1: Voltage recovery time under various scenarios [67]

Trip Function	Default settings		Allowable settings	
	Voltage (pu)	Recovery time (s)	Voltage (pu)	Recovery time (s)
Under-voltage 2 (UV2)	0.45	0.16	0.0 – 0.50	0.16 – 2.0
Under-voltage 1 (UV1)	0.70	2.0	0.0 – 0.88	2.0 -21.0
Over-voltage 1 (OV1)	1.10	2.0	1.10 – 1.20	1.00 -13.0
Over-voltage 2 (OV2)	1.20	0.16	Fixed at 1.20	Fixed at 0.16

The default values of listed recovery times may vary across different utilities. The permissible settings for such variations are also listed in Table 3.1. Considering the most rigorous case, voltage at the PCC of DER unit must return to 0.88 pu of the pre-fault value within 2 s of the fault to avoid tripping.

## 3.2 Proposed Methodology

A methodology is developed in this section for the placement of SVC based on reactive power margin to enhance post-fault voltage recovery behavior at the PCC of DERs in an islanded microgrid. To this end, the relevant calculation procedures and modeling are explained at first. Then the proposed framework is step-wise presented.

### 3.2.1 Load Flow Calculation

Load flow calculation has to be done at the beginning to set preconditions for dynamic simulations. For this purpose, Newton-Raphson Method is applied. Load flow problem basically deals with a set of nonlinear equations. There are multiple ways to solve a set of nonlinear equations with a number of unknown variables. Newton-Raphson Method is an effective technique for it, which uses an iterative way to solve the nonlinear equations.

Generally, the apparent power at  $i$ -th bus can be expressed as follows.

$$S_i = P_i + j Q_i = V_i \sum_{k=1}^n V_{ik} V_k \quad (3.1)$$

$$S_i = \sum_{k=1}^n V_{ik} V_k Y_{ik} \angle(\delta_i - \delta_k - \theta_{ik}) \quad (3.2)$$

The bus injected real power ( $P_i$ ) and reactive power ( $Q_i$ ) of  $i$ -th bus can be expressed as follows.

$$P_i = \sum_{k=1}^n V_{ik} V_k Y_{ik} \cos(\delta_i - \delta_k - \theta_{ik}) \quad (3.3)$$

$$Q_i = \sum_{k=1}^n V_{ik} V_k Y_{ik} \sin(\delta_i - \delta_k - \theta_{ik}) \quad (3.4)$$

Equation (3.3) and (3.4) can be written as

$$P_i = V_i V_i Y_{ii} \cos\theta_{ii} + \sum_{\substack{k=1 \\ k \neq i}}^n V_i V_k Y_{ik} \cos(\delta_i - \delta_k - \theta_{ik}) \quad (3.5)$$

$$Q_i = -V_i V_i Y_{ii} \sin\theta_{ii} + \sum_{\substack{k=1 \\ k \neq i}}^n V_i V_k Y_{ik} \sin(\delta_i - \delta_k - \theta_{ik}) \quad (3.6)$$

Where,  $V_i$  and  $V_k$  are voltage magnitude of  $i$ -th and  $k$ -th bus respectively,  $Y_{ik}$  is the magnitude of  $ik$ -th element of bus admittance matrix (i.e.  $Y_{bus}$ ),  $\delta_i$  and  $\delta_k$  is the voltage angle of  $i$ -th and  $k$ -th bus and  $\theta_{ik}$  is the angle of  $ik$ -th element of  $Y_{bus}$ .

$$\text{According to Newton-Raphson method, } \Delta f = J \Delta X \quad (3.7)$$

If

$$\Delta P_i = P_{i \text{ (sp)}} - P_{i \text{ (cal)}} \quad (3.8.)$$

Then  $I = 1, 2, 3, \dots, n, I \neq \text{slack}$ , and if

$$\Delta Q_i = Q_{i \text{ (sp)}} - Q_{i \text{ (cal)}} \quad (3.9)$$

Where, sp and cal denotes the specified and calculated values respectively, then equation (3.9) can be written as

$$\begin{bmatrix} \Delta P \\ \Delta Q \end{bmatrix} = \begin{bmatrix} H & N \\ M & L \end{bmatrix} \begin{bmatrix} \Delta \delta \\ \Delta V \end{bmatrix} \quad (3.10)$$

$$\Delta P_i^{(r)} < \varepsilon, \Delta Q_i^{(r)} < \varepsilon$$

The off diagonal and diagonal elements of the sub matrices H, N, M and L are determined by differentiating equation (3.3) and (3.4) with respect to  $\delta$  and  $|V|$ .



The following flow chart shows the steps to solve the load flow solution using Newton-Raphson method.

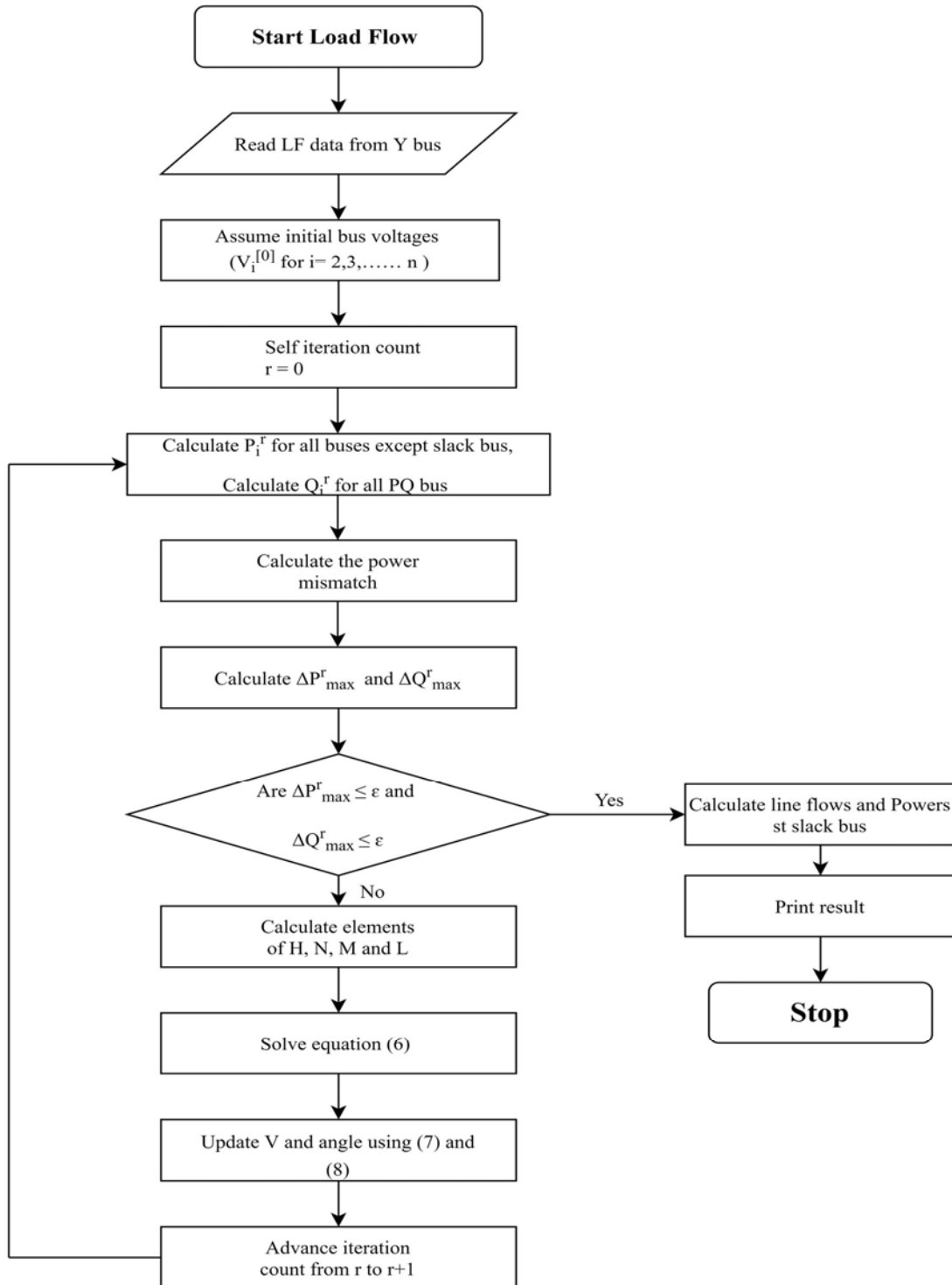


Figure 3.1: Flowchart of load flow calculation

### 3.2.2 Reactive Power Margin

The demand and the lack of new generation and transmission networks have forced power systems to operate closer to their safety limits. Additionally, due to distributed generators penetration, distribution networks are becoming more vulnerable to voltage instability problems. Therefore, a reliable voltage stability index is needed which can help to measure system stability. Reactive power margin is considered as a reliable voltage stability index for a power system [68]. The reactive power margin is the difference between the maximal reactive load that can be consumed in a bus and the corresponding load at the initial operating condition. It can be measured from the Q-V curve of the bus as shown in Figure 3.2. It is the distance of the lowest point of the curve from the horizontal axis.

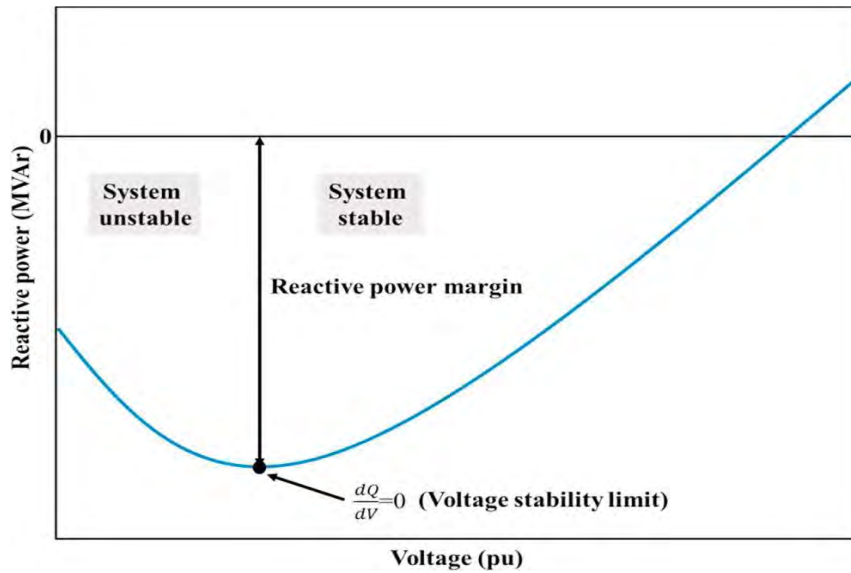


Figure 3.2: Reactive power margin [68]

Q-V curve is constructed using the continuation method by increasing reactive power load while keeping the real power load constant. The bottom of Q-V curve specifies the stability limit or collapse point of the system as V-Q sensitivity reaches infinity at this point.

Therefore, the Q margin of i-th bus can be measured from the equation below.

$$Q_i^{margin} = Q_i^* - Q_i^o \quad (3.11)$$

Where  $Q_i^{margin}$  denotes the reactive power margin of  $i^{th}$  bus,  $Q_i^*$  and  $Q_i^o$  denote the reactive power consumption at collapse and base operation points for  $i^{th}$  bus, respectively.

### 3.2.3 Load Modeling

Load can be modeled in various ways depending on their dependence on voltage and frequency. Conventionally, loads can be classified as constant power, constant current and constant impedance type loads or a combination of them. In this thesis, the most widely used exponential load model is used [69]. In this study, the main focus is voltage stability. Therefore, the frequency dependent load model is not taken into account.

In the voltage dependent exponential load model, the active and reactive power can be expressed by the following equations.

$$P_L = P_o (V/V_o)^a \quad (3.12)$$

$$Q_L = Q_o (V/V_o)^b \quad (3.13)$$

where  $a$  and  $b$  are the load exponents,  $P_L$  is the active power injection,  $Q_L$  is the reactive power injection and  $V$  is the bus voltage. Also,  $P_o$ ,  $Q_o$  and  $V_o$  are the nominal values of the active and reactive power injections and the voltage magnitude, respectively. If  $a=0$  and  $b=0$ , both real and reactive power are presented by constant power load models. If  $a=1$  and  $b=1$ , both real and reactive power are presented by constant current load models. If  $a=2$  and  $b=2$ , both real and reactive power are presented by constant impedance load models.

### 3.2.4 Steps of the SVC Placement Algorithm

Based on the reactive power margin, an algorithm is proposed for SVC placement to mitigate the cascading tripping of DERs. For better understanding, the steps are illustrated via a flowchart in Figure 3.3. The steps are described as follows.

- Step 1 – Execution of time domain simulation: With the application of various faults in the system, time domain simulations are carried out to check post-fault voltage recovery profiles at the PCCs of DERs. As the three phase faults are considered to be the most severe faults, present study concentrates on voltage recovery with a three-phase fault near the generator bus. This makes the proposed methodology applicable for all other fault types. In addition, various load models are consecutively taken into account during dynamic (i.e. time domain) simulations.

- Step 2 – Identification of grid code compliancy: In this stage, compliance of the post-fault voltage recovery performance with the given the acceptable grid code (e.g., IEEE Standard 1547-2018) is checked. If **yes** (i.e., the compliance is met), the process terminates in Step-8. Else, it indicates that DERs are under a possible risk of incurring cascading tripping. Therefore, the framework switches to Step 3 for further measures.
- Step 3 – Calculation of reactive power margin: In this step, the reactive power margin  $Q_i^{margin}$  of each bus is calculated using equation 3.11.
- Step 4 – Centralized placement of a single SVC unit: The bus with the lowest reactive power margin is chosen for a centralized SVC placement since this bus is the most vulnerable to voltage instability. The rating of SVC is decided based on the values of post-fault voltage and reactive power margin.
- Step 5 – Identification of grid code compliance with centralized SVC: In this stage, further examination is done to identify whether the post-fault voltage recovery performance with centralized placement of SVC meets the grid code requirement. If **yes**, the workflow proceeds to Step 8 to conclude the process. Else, it indicates that a centralized placement of SVC is not sufficient to avert the cascading tripping of DERs. Hence, the algorithm switches to Step 6 for distributed placement of SVC.
- Step 6 – Distributed placement of multiple SVC: In distributed placement approach, SVCs are dispersed on multiple buses that have relatively lower values of reactive power margin. In addition to the placement of a SVC at the bus with the lowest reactive power margin, a second SVC unit is connected to the bus with next lowest reactive power margin.
- Step 7 – Identification of grid code compliancy with distributed SVC: In this stage, examination is carried out to find if the voltage recovery with current distributed SVC placement is satisfactory. If **yes**, the workflow jumps to Step 8 to conclude the process. Else, it again proceeds to Step 6 for further placement of distributed SVC unit in the next lowest reactive power margin. This procedure is repeated until the voltage recovery of all DER buses become acceptable as specified by the grid code.
- Step 8 – Completion of algorithm: The SVC placement algorithm is completed.

Note that before placing SVC in a microgrid, the proposed methodology is executed to find the most appropriate location. In a specific microgrid, either the centralized or the distributed SVC placement strategy is eventually adopted.

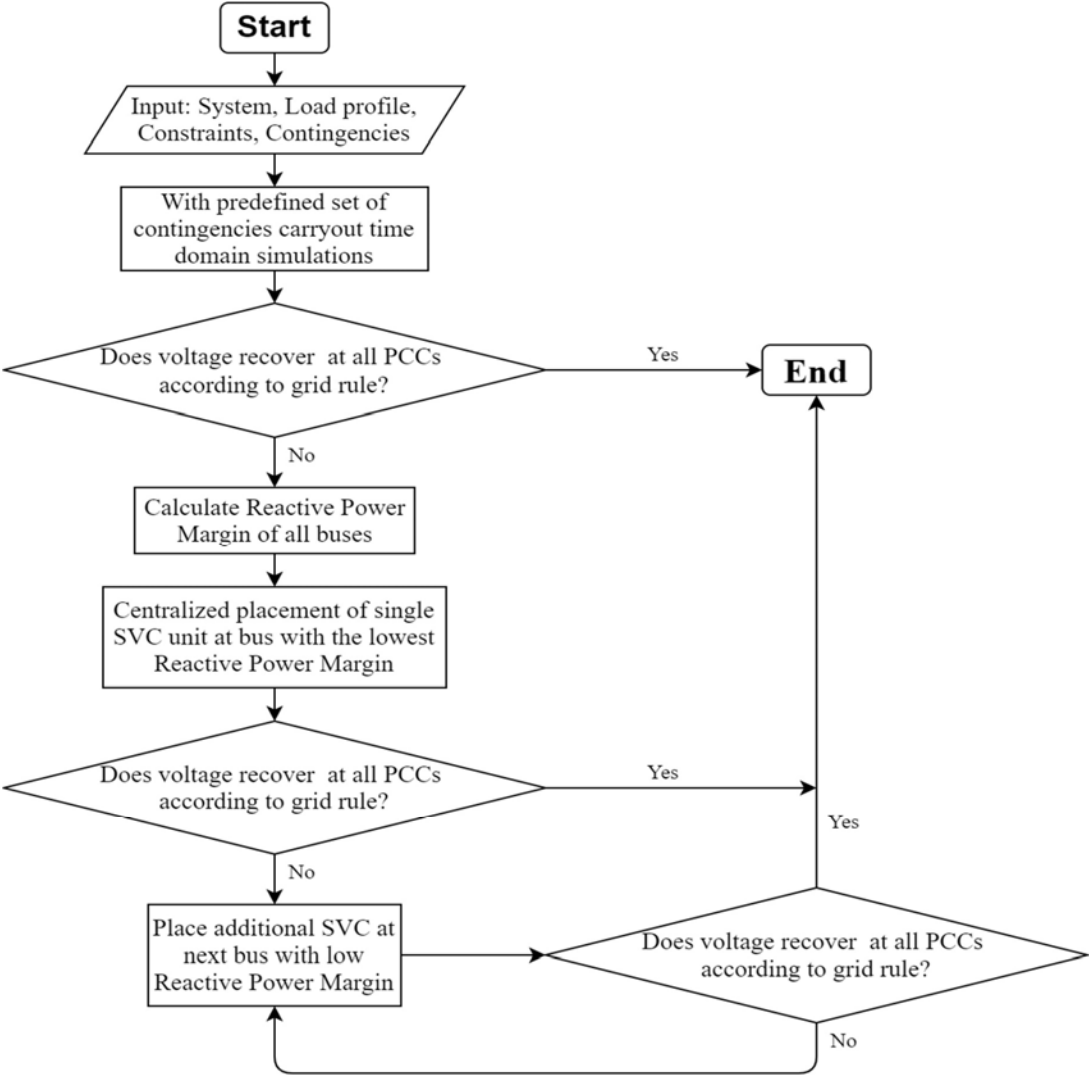


Figure 3.3: Flow chart of the proposed SVC placement algorithm

In the next chapter, detailed simulations are carried out to examine the effectiveness of the proposed methodology.

# CHAPTER 4

## Results and Discussions

## 4.1 Introduction

In this chapter, simulation results are presented in detail. At first, the test network and simulation platform are described. Then, the proposed methodology is applied to the test network to verify its effectiveness. Various renewable penetration cases are considered for this purpose. Besides, the impact of load modeling on the performance of the proposed technique is explored. Finally, the developed methodology is compared to an existing approach for validation.

## 4.2 Test System and Simulation Tool

All the simulations are performed using Digisilent Powerfactory 15.1 [70], which is a widely accepted simulation software to perform power system studies. A slightly modified IEEE 43 bus industrial network [71] is taken as the test microgrid. A detailed model of a renewable-integrated microgrid was constructed, in which solar photovoltaic, wind and diesel based DER units are utilized. The microgrid consists of both static and rotating (i.e. induction motors) loads. The test network has a total load of 23.38 MW with a VAR consumption of 10.98 MVAR.

The total demand is supplied by 4 DER units. The DER units consist of two Diesel Generators (DG), one Wind Turbine (WT) and a solar Photovoltaic (PV) array. The two DGs are connected at bus 4 and bus 100 while the WT is connected at bus 50 and the PV array is connected at bus 41. The location of the DERs are shown in Table 4.1 below.

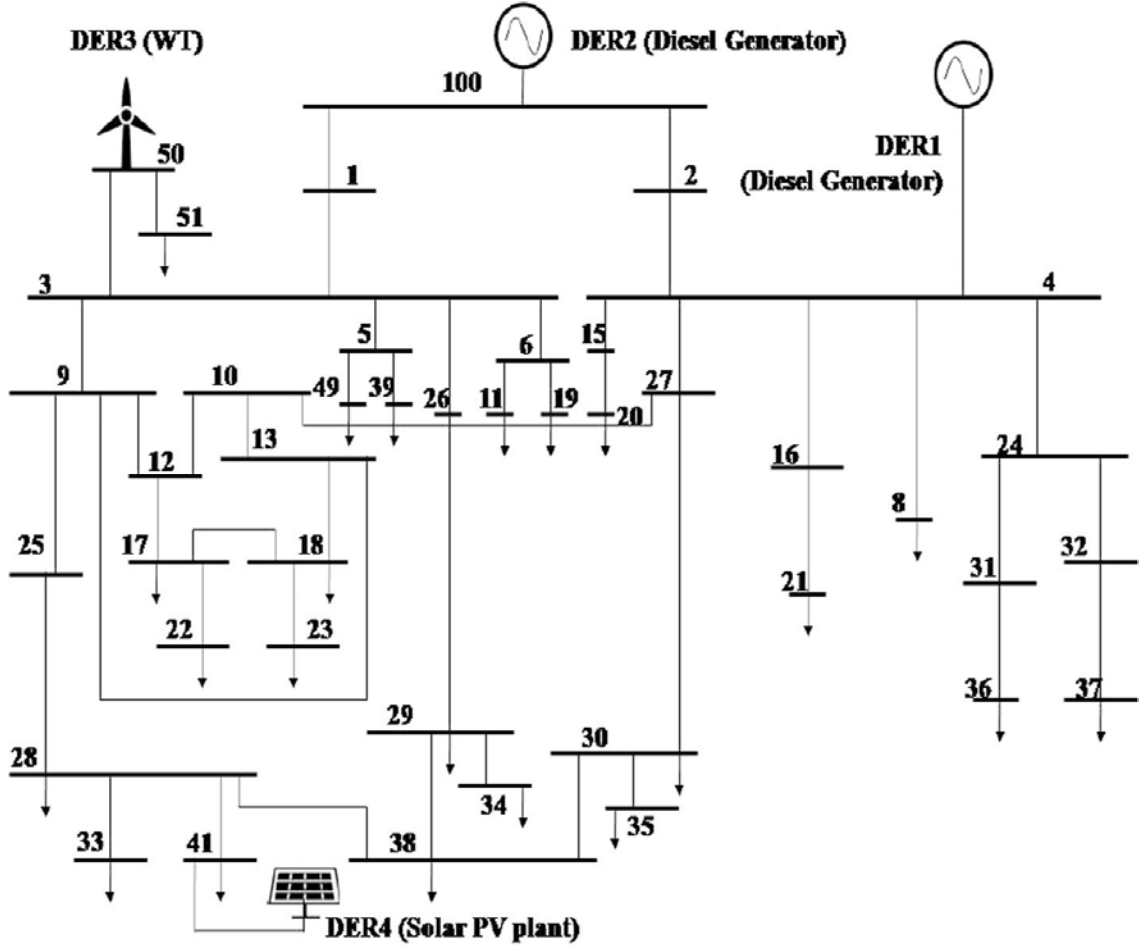


Figure 4.1: Single line diagram of the test microgrid [42]

Table 4.1: Types and location of DER units

Distributed generator	Fuel type	Location
DER1	Diesel generator	Bus 4 (PCC1)
DER2	Diesel generator	Bus 100 (PCC2)
DER3	Wind turbine	Bus 50 (PCC3)
DER4	PV array	Bus 41 (PCC4)

### 4.3 Calculation of Reactive Power Margin

The values of reactive power margin in various load buses are calculated using equation (3.11). The reactive power margin of the five most vulnerable buses is shown in Table 4.2.

Table 4.2: Reactive power margin of five most vulnerable buses

Bus number	Reactive power margin (MVAR)
21	2.94
37	3.88
22	4.55
38	5.01
41	5.44

It can be seen that bus 21 is found to be the most vulnerable bus as it has the lowest reactive power margin. Furthermore, bus 37, bus 22, bus 38 and bus 41 are the other four buses with consecutive lowest reactive power margin.

### 4.4 Simulation Scenarios

Five simulation cases are investigated in this chapter. To build different cases, the RE penetration level is varied from 23% to 50%. The total apparent power is assumed to be unchanged to 26 MVA in all cases. The RE penetration level is defined as the ratio between the total renewable generation (i.e. combined power generation from DER3 and DER4) and total generation (i.e. combined power generation from DER1, DER2, DER3 and DER4). Table 4.3 outlines the simulation scenarios.

Table 4.3: Simulation cases

Case no.	DER1 (MVA)	DER2 (MVA)	DER3 (MVA)	DER4 (MVA)	RE penetration level (%)
Case-1	10	10	5	1	23
Case-2	10	8.2	5	2.8	30
Case-3	10	5.6	5	5.4	40
Case-4	10	4.3	6	5.7	45
Case-5	7	6	7	6	50



Among different types of fault, three phase fault is considered to be the most severe one. To simulate this most severe condition, a three-phase fault with an impedance of  $j0.1 \Omega$  is applied at bus 31 at 1s. The fault was cleared after 10 cycles.

## 4.5 Simulation Results and Analyses

In this sub-section, simulation results are presented and analyzed in detail for various renewable penetration cases. All loads are assumed to be constant impedance loads.

### 4.5.1 Case-1: 23% RE Penetration

According to the adopted grid code, the voltage at the DER PCC should return to 0.88 p.u. of the pre-fault value within 2s of the fault to avert DER tripping. Note that sequential tripping of DER units due to unsatisfactory voltage recovery is taken into account to match the realistic operational practice of a power system.

It is found from time-domain simulations that the voltage at PCC1 (i.e. at bus 4) is found to be 0.8189 p.u. as shown in Figure 4.2. Therefore, the post-fault voltage recovery performance at PCC1 is unsatisfactory. Consequently, DER1 trips, which is evident from its power output curve shown in Figure 4.3.

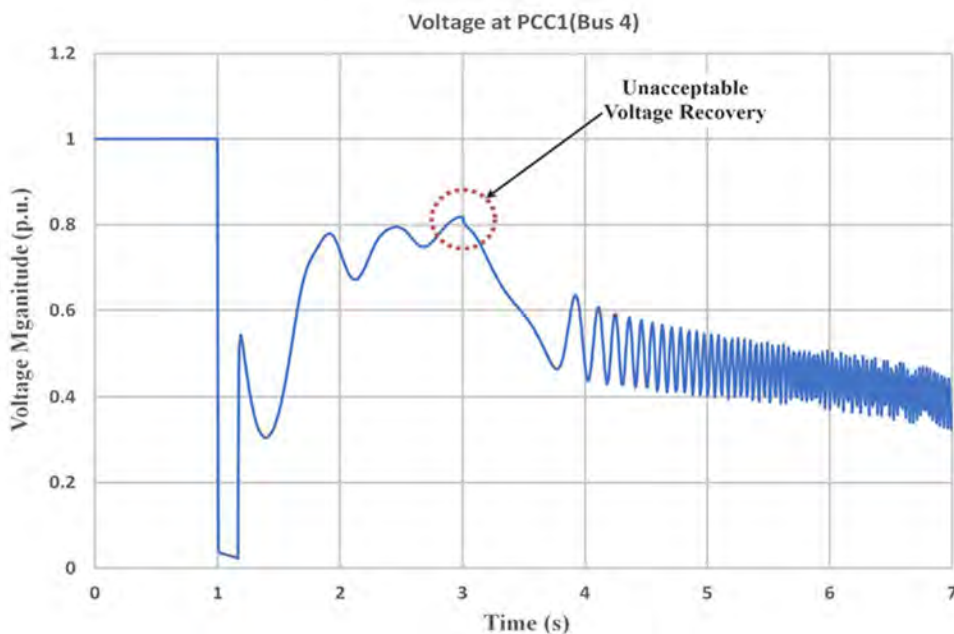


Figure 4.2: Voltage at PCC1 (Bus 4) at 23% RE penetration

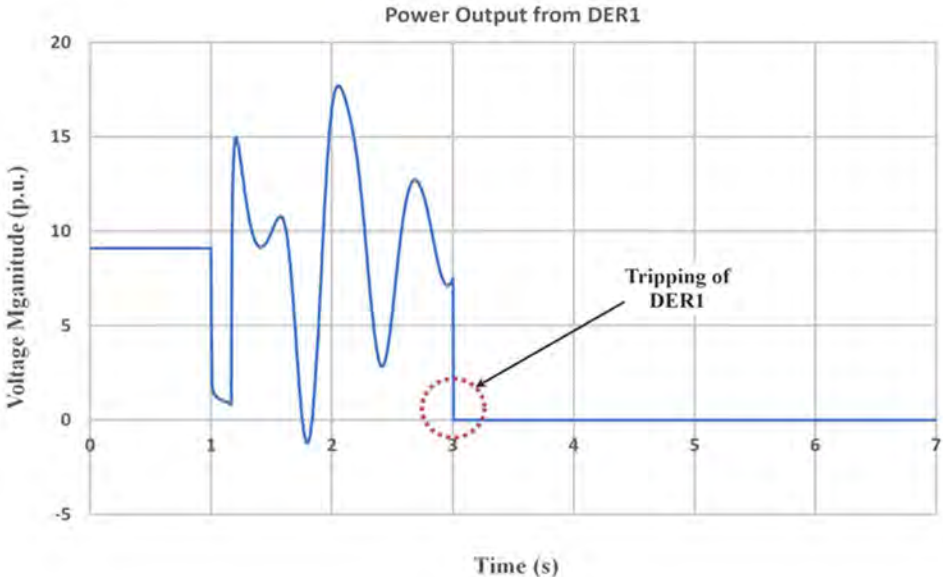


Figure 4.3: Power output from DER1 at 23% RE penetration

Tripping of DER1 causes reduction of reactive support that result in further deterioration of voltage recovery performance. For instance, Figure 4.4 shows the voltage profile at PCC4. As the post-fault voltage recovery is unsatisfactory, DER4 trips. The power output curve of DER4 is provided in Figure 4.5.

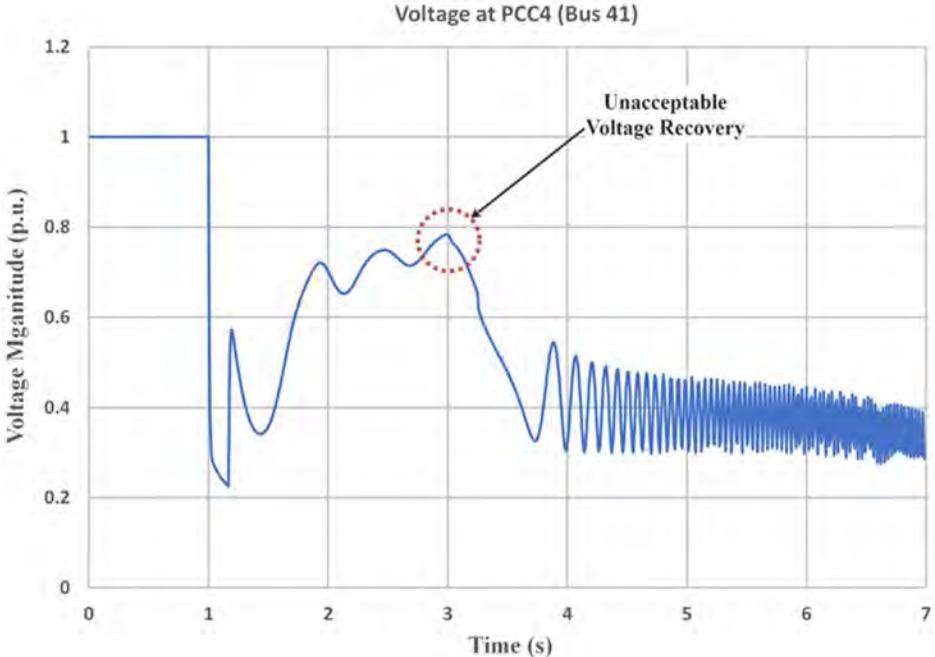


Figure 4.4: Voltage at PCC4 (Bus 41) at 23% RE penetration

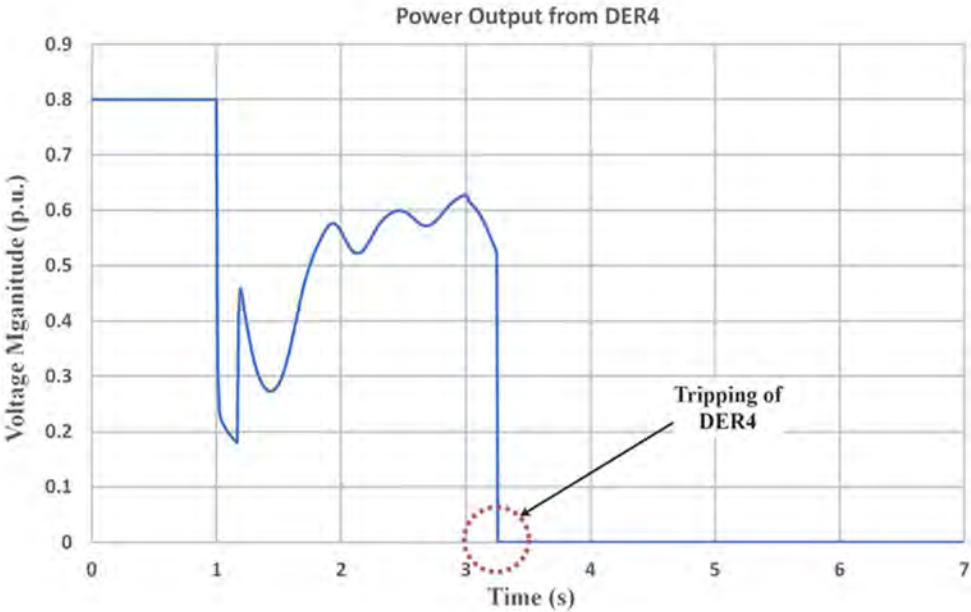


Figure 4.5: Power output from DER4 at 23% RE penetration

The consecutive tripping of two DER units worsens the post-fault recovery performance at PCC3 as shown in Figure 4.6. It initiates the tripping of the DER3 as shown by Figure 4.7.

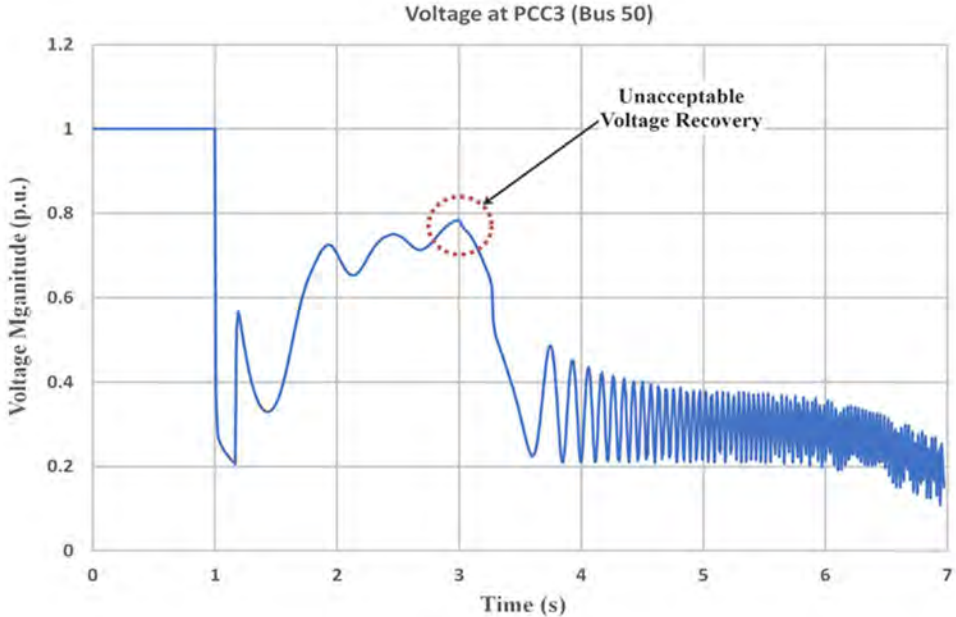


Figure 4.6: Voltage at PCC3 (Bus 50) at 23% RE penetration

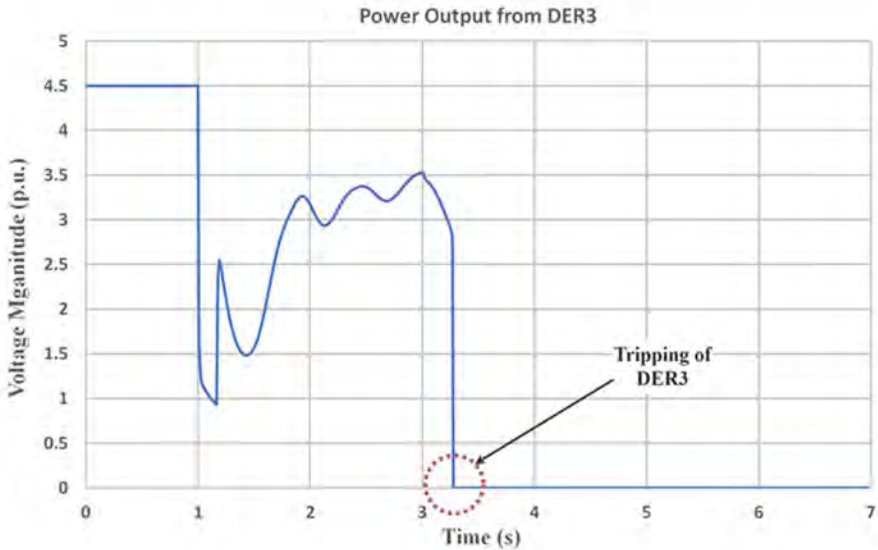


Figure 4.7: Power output from DER3 at 23% RE penetration

Due to the of the tripping of the three DERs, poor voltage recovery performance is observed at PCC2 as shown in Figure 4.8. It causes the tripping of DER2, which is shown in Figure 4.9.

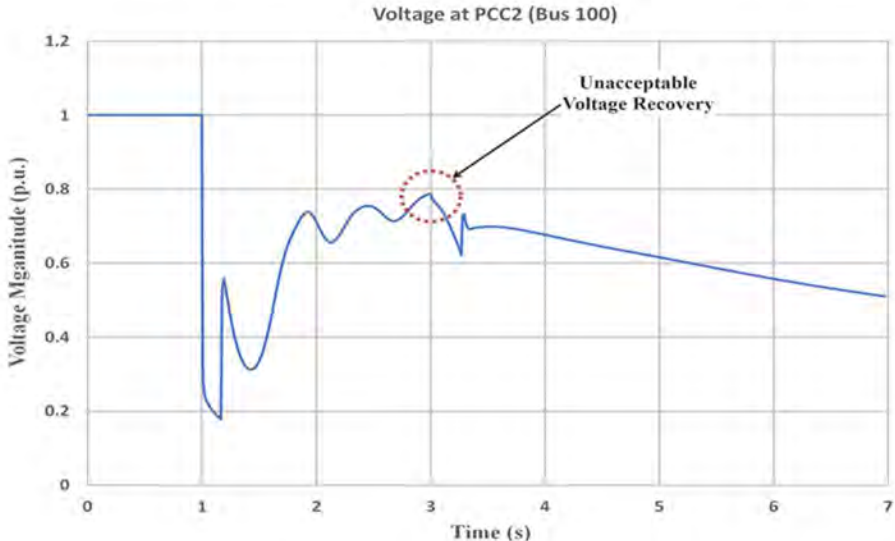


Figure 4.8: Voltage at PCC2 (Bus 100) at 23% RE penetration

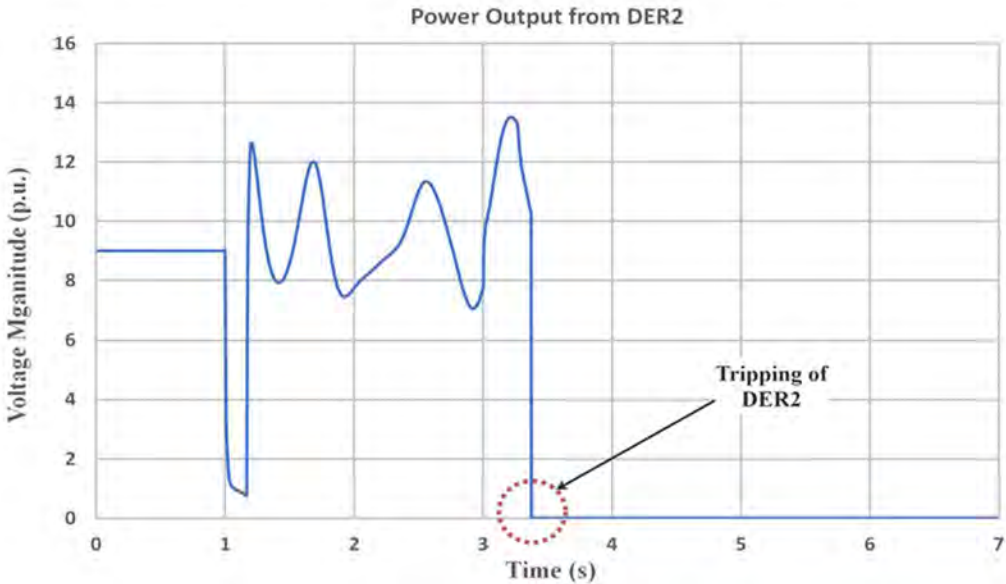


Figure 4.9: Power output from DER2 at 23% RE penetration

It is found from above simulations that cascading tripping of all DER units takes place in the microgrid. As a result, the whole microgrid encounters a blackout. Occurrence of this blackout is revealed by the collapse of motor speed at bus 37, which is depicted in Figure 4.10. Note that motor speed at bus 37 is taken as an example case to realize the blackout. For other motors, same phenomenon is observed.

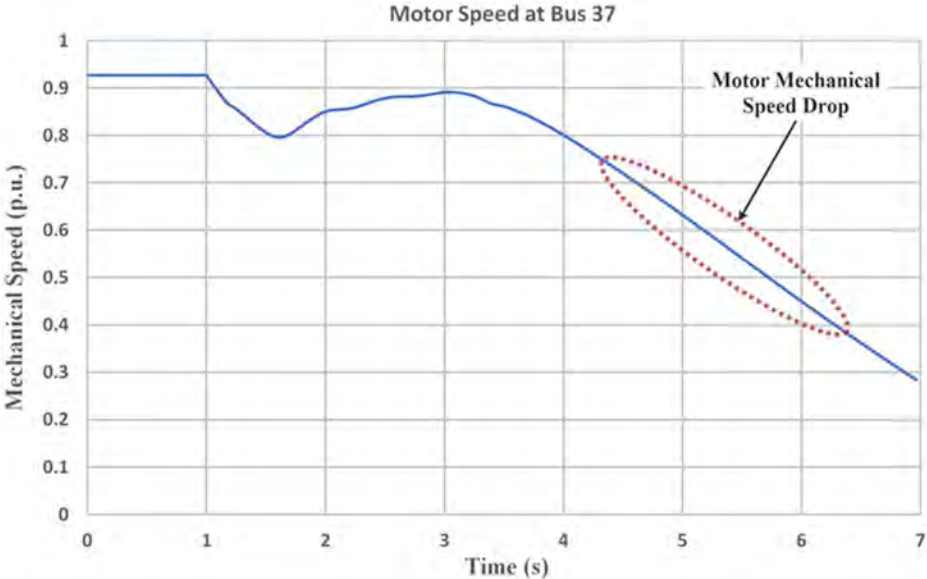


Figure 4.10: Motor speed at bus 37 (indication of blackout) at 23% RE penetration

In order to prevent the blackout at 23% RE penetration level, a SVC is connected at bus 21 according to the proposed algorithm. The rating of this SVC is 2.07 MVAR, which is intuitively determined from the time domain simulations and the value of reactive power margin. With the placement of such centralized SVC, the post-fault voltage recovery performances of all DER units become satisfactory. The voltage curves of different DERs are shown in Figure 4.11 to 4.14.

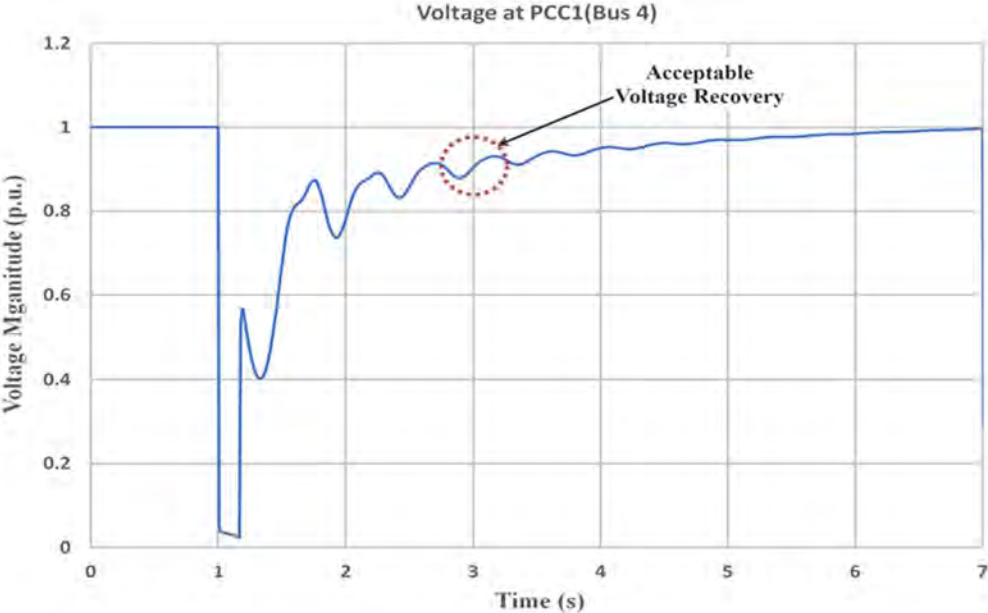


Figure 4.11: Voltage at PCC1 (Bus 4) at 23% RE penetration with SVC

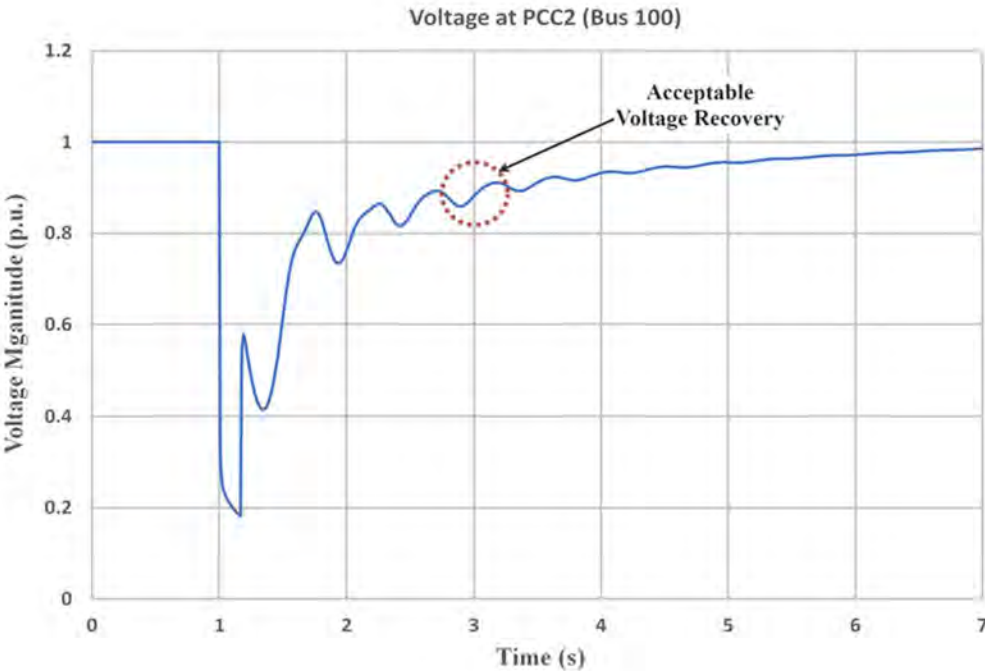


Figure 4.12: Voltage at PCC2 (Bus 100) at 23% RE penetration with SVC

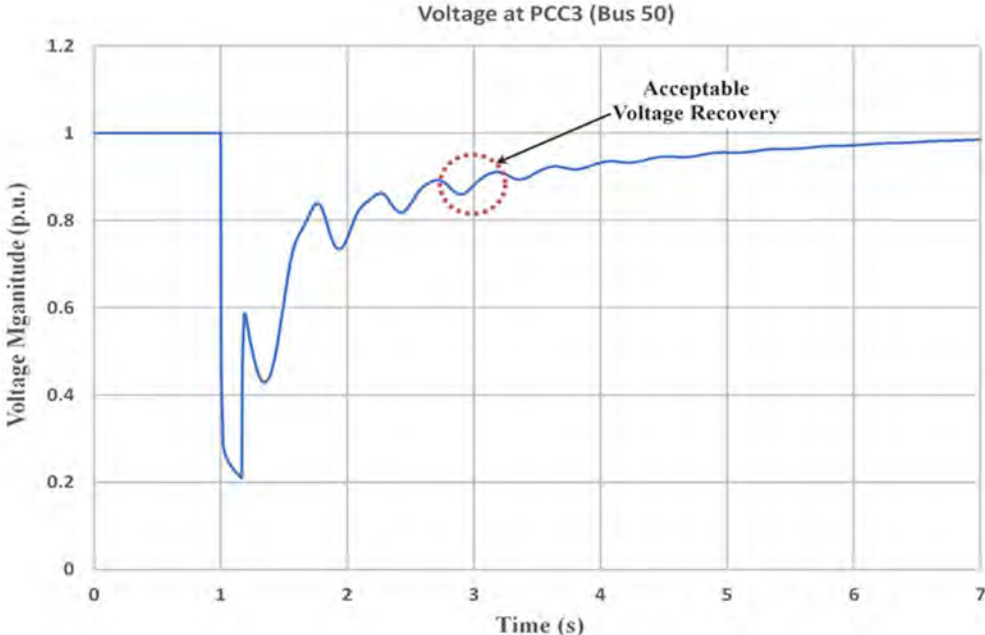


Figure 4.13: Voltage at PCC3 (Bus 50) at 23% RE penetration with SVC

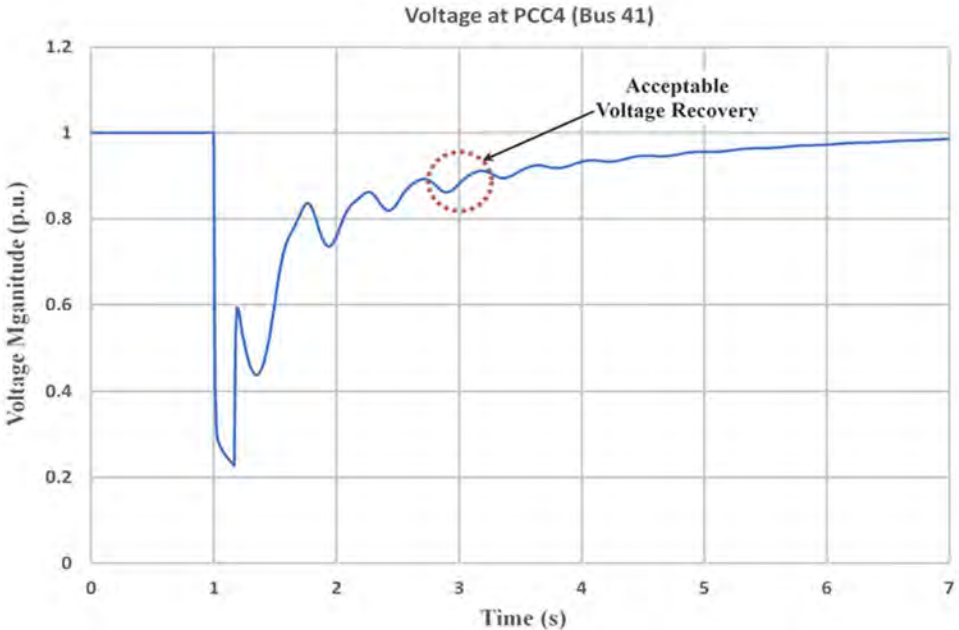


Figure 4.14: Voltage at PCC4 (Bus 41) at 23% RE penetration with SVC

The voltage magnitude after 2s of fault application is summarized in Table 4.4. It can be clearly seen that due to the proposed SVC placement algorithm, the post-fault voltages at all DER units become more than 0.88 p.u. As a result, no cascading tripping of DERs take place, the risk of blackout is mitigated.

Table 4.4: Post-fault voltage with SVC after 2s of fault occurrence at 23% RE penetration

PCC	Voltage magnitude (p.u.)
PCC1(Bus 4)	0.9029
PCC2(Bus 100)	0.8806
PCC3(Bus 50)	0.8804
PCC4(Bus 41)	0.8807

**4.5.2 Case-2: 30% RE Penetration**

In this case, renewable sources supply 7.8 MVA out of 26 MVA generation in the microgrid. According to the grid standard, the voltage at the DER PCC has to return to 0.88



p.u. within 2s of the fault application to avoid DER tripping. However, the voltage at PCC1 (i.e. at bus 4) is found to be 0.303 p.u. as shown in Figure 4.15. Therefore, voltage recovery of DER1 is unsatisfactory. As a result, DER1 trips, which is depicted by its power output curve shown in Figure 4.16.

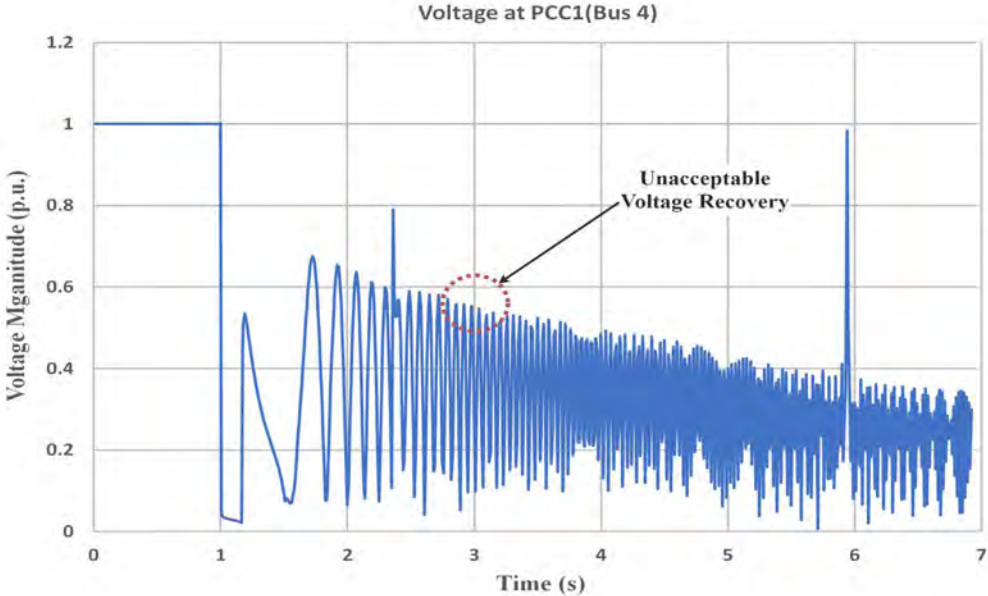


Figure 4.15: Voltage at PCC1 (Bus 4) at 30% RE penetration

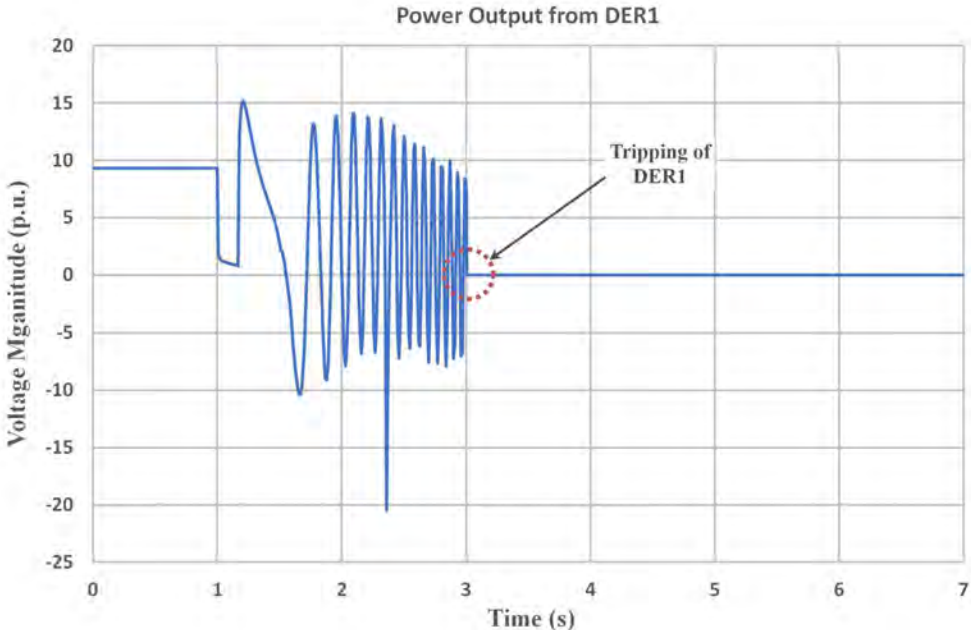


Figure 4.16: Power output from DER1 at 30% RE penetration

Due to tripping of DER1, reactive power support in the microgrid decreases. It causes further deterioration of voltage recovery enactment. For example, Figure 4.17 shows the

voltage profile at PCC4 (i.e. Bus 41). It can be seen that the post-fault voltage of DER4 is unacceptable. As such, DER4 trips, which is evident by its power output curve illustrated in Figure 4.18.

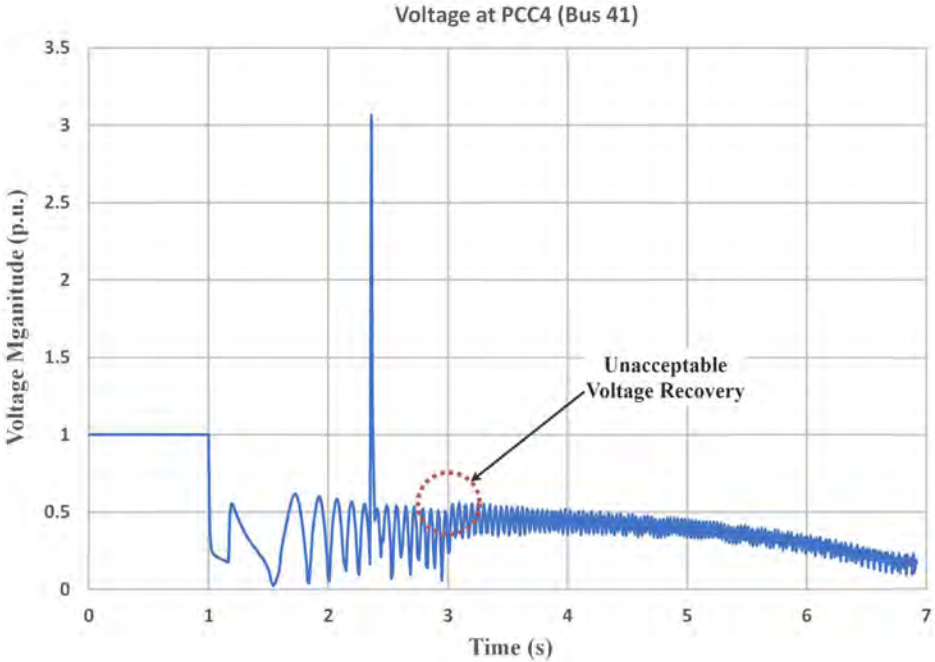


Figure 4.17: Voltage at PCC4 (Bus 41) at 30% RE penetration

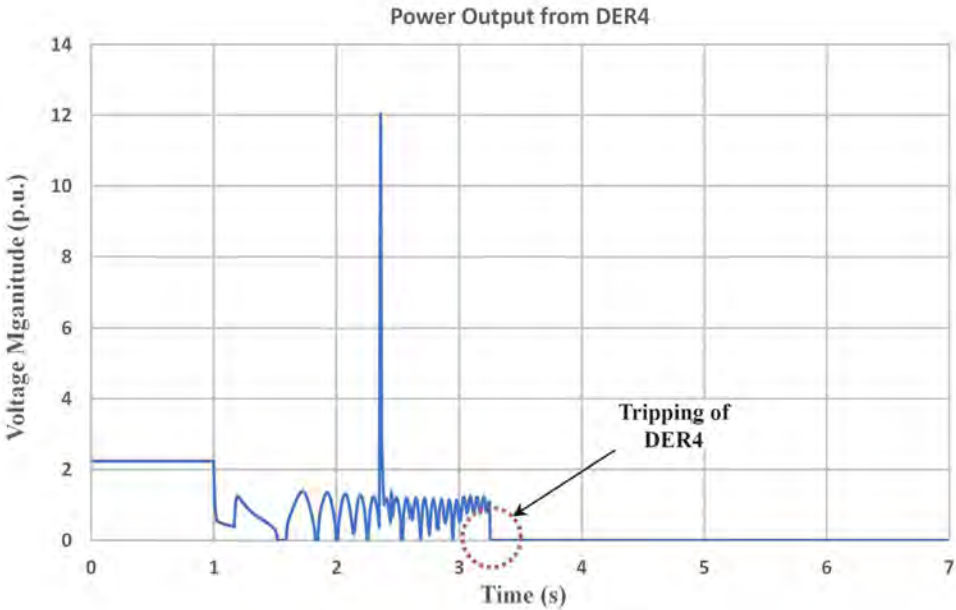


Figure 4.18: Power output from DER4 at 30% RE penetration

The successive tripping of two DER units deteriorates the post-fault recovery performance at PCC3 as depicted in Figure 4.19. It instigates the tripping of the DER3 as shown by Figure 4.20.

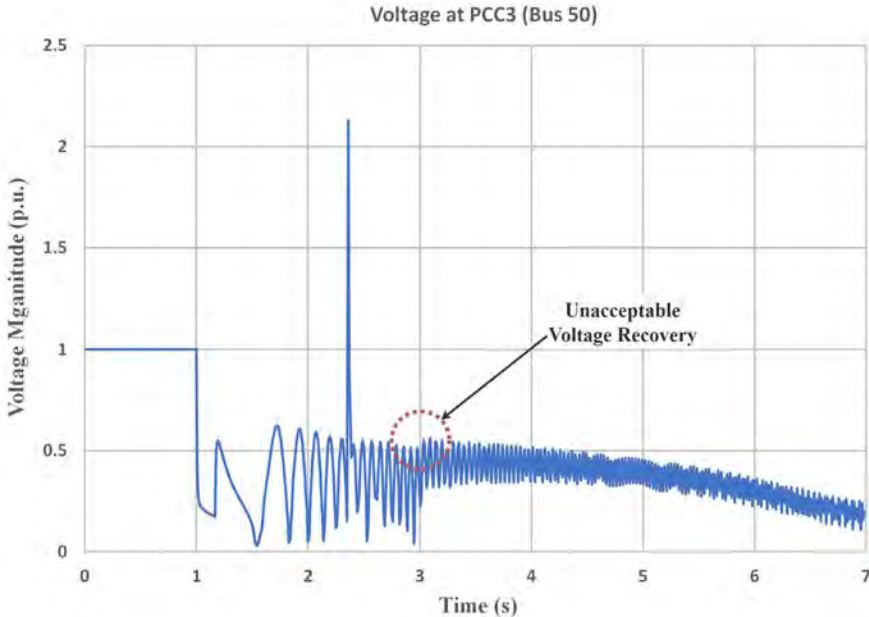


Figure 4.19: Voltage at PCC3 (Bus 50) at 30% RE penetration

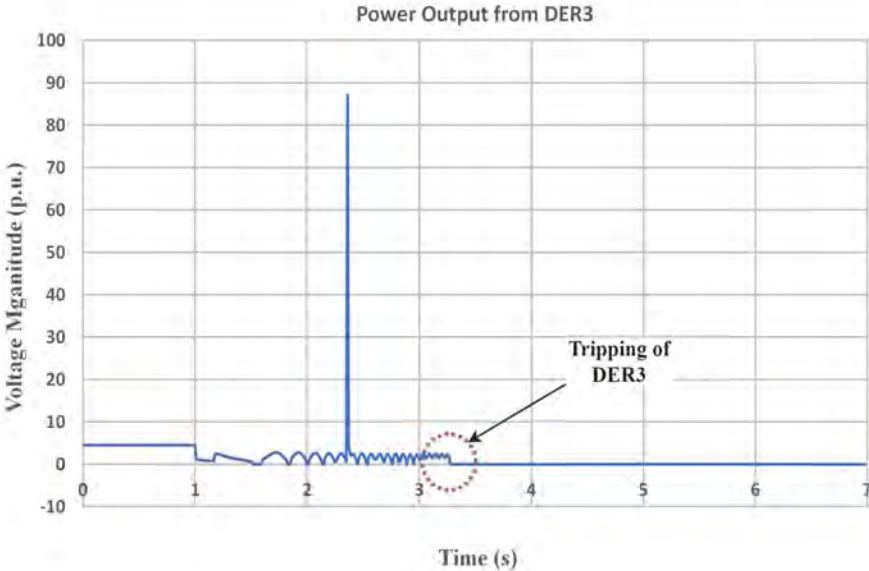


Figure 4.20: Power output from DER3 at 30% RE penetration

Due to the tripping of the three DERs, unacceptable voltage recovery performance is attained at PCC2 as shown in Figure 4.21. It causes the tripping of DER2, which is shown in Figure 4.22.

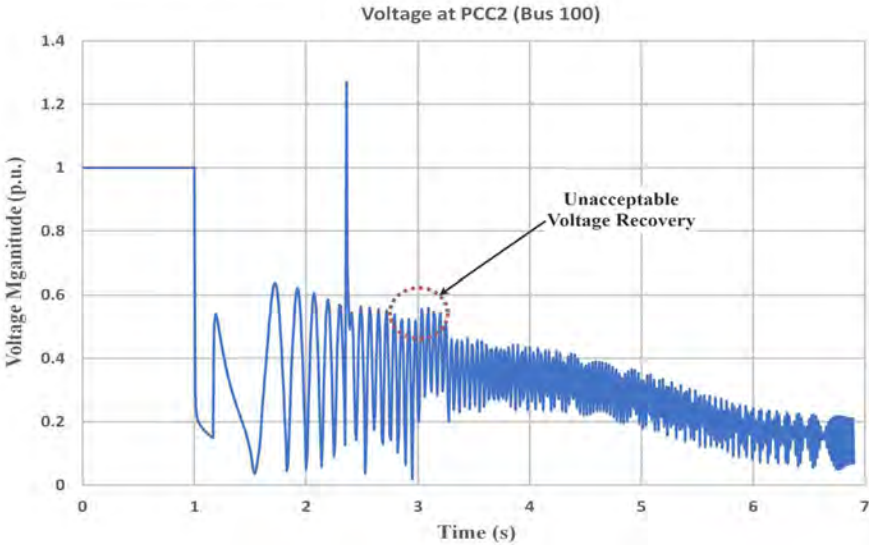


Figure 4.21: Voltage at PCC2 (Bus 100) at 30% RE penetration

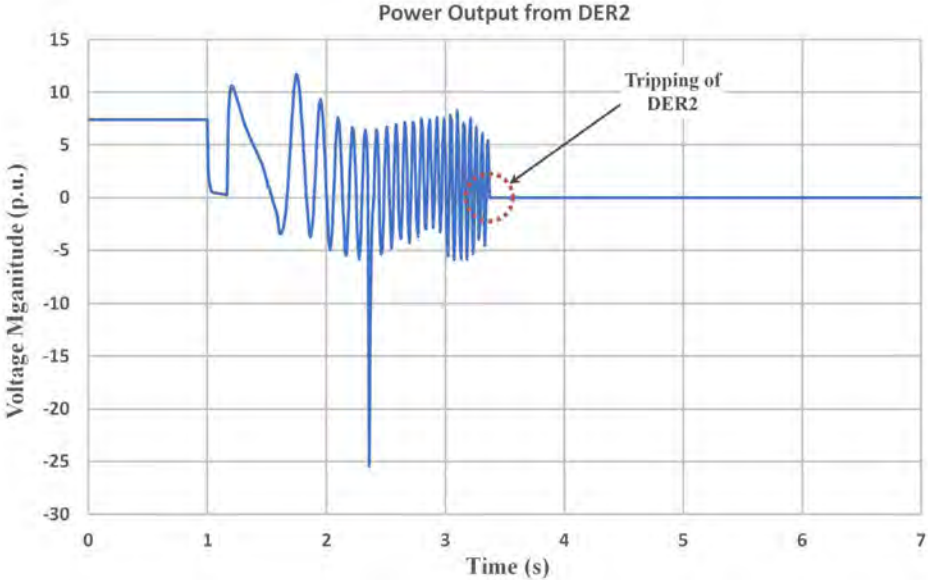


Figure 4.22: Power output from DER2 at 30% RE penetration

It is noticed from above simulations that cascading tripping of all DER units occur. Consequently, the entire microgrid incurs a blackout. This blackout is revealed by the collapse of motor speed at bus 37, which is depicted in Figure 4.23.

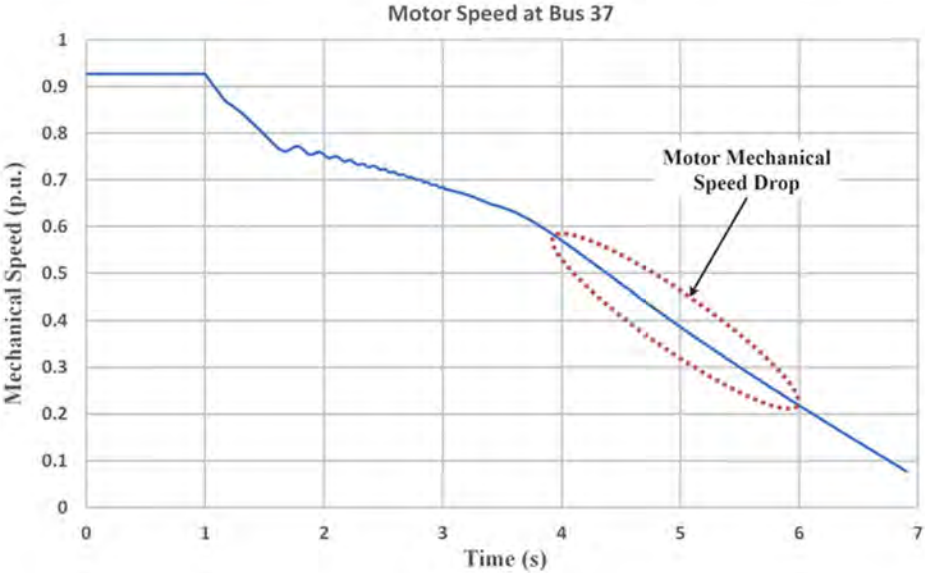


Figure 4.23: Motor speed at bus 37 (indication of blackout) at 30% RE penetration

To avert the blackout at 30% RE penetration case, a SVC is placed at bus 21 using the proposed algorithm. The rating of this SVC is 2.35 MVAR, which is found based on the time domain simulations and the value of reactive power margin. Due to the placement of this centralized SVC, the post-fault voltage recovery performances of all DER units are found to be satisfactory. The voltage curves of different DERs are shown in Figure 4.24 to 4.27.

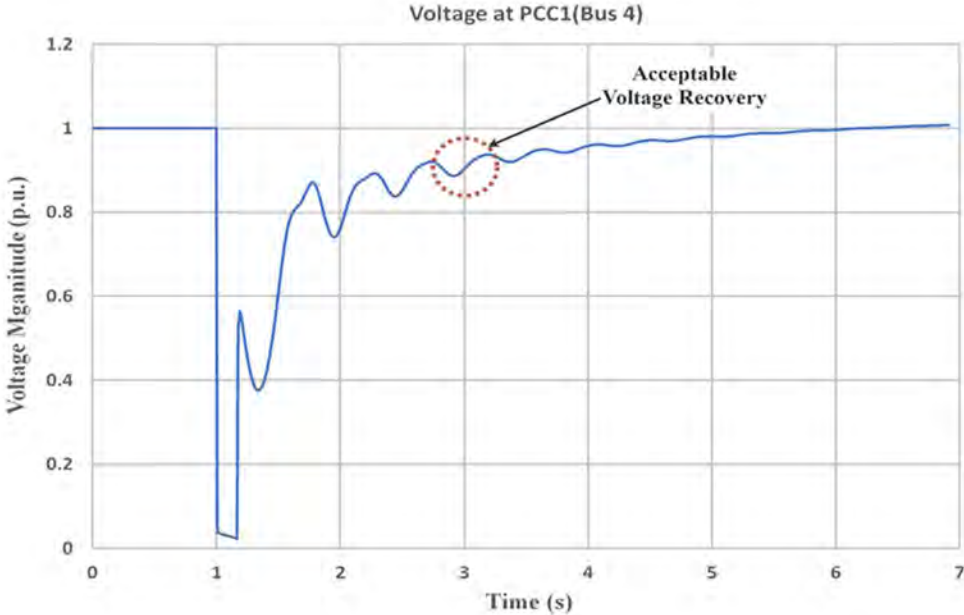


Figure 4.24: Voltage at PCC1 (Bus 4) at 30% RE penetration with SVC

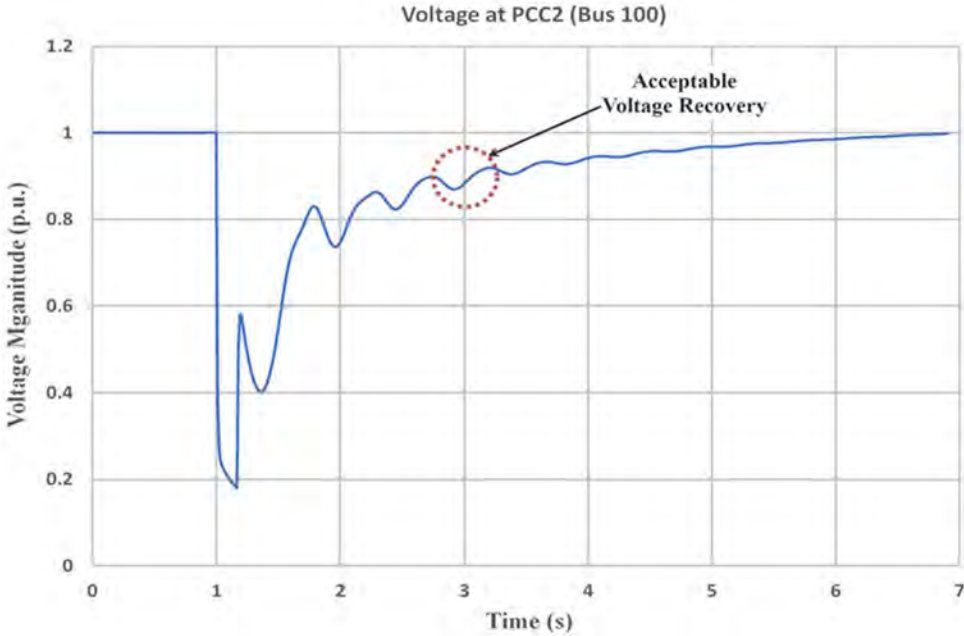


Figure 4.25: Voltage at PCC2 (Bus 100) at 30% RE penetration with SVC

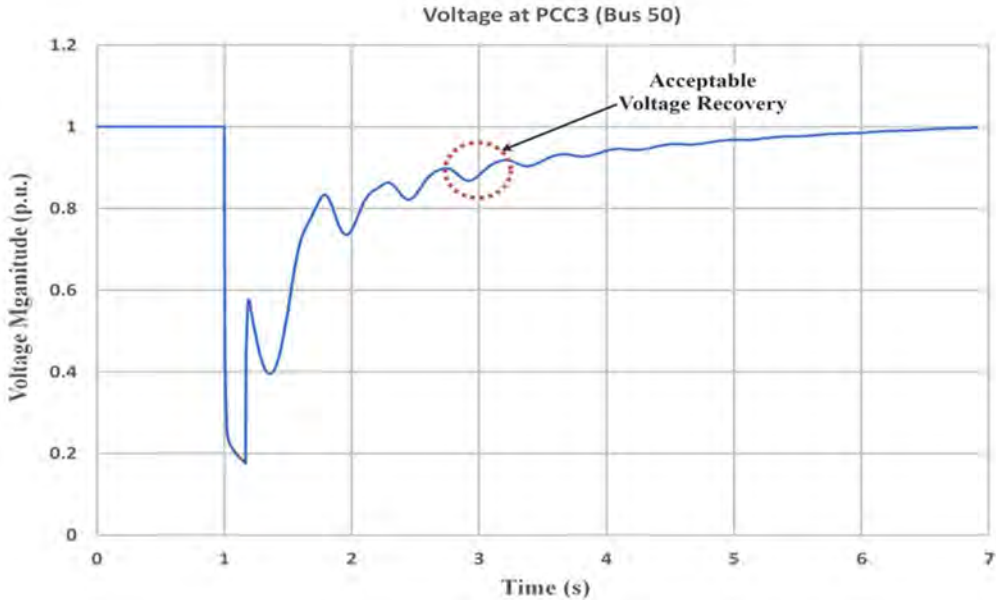


Figure 4.26: Voltage at PCC3 (Bus 50) at 30% RE penetration with SVC

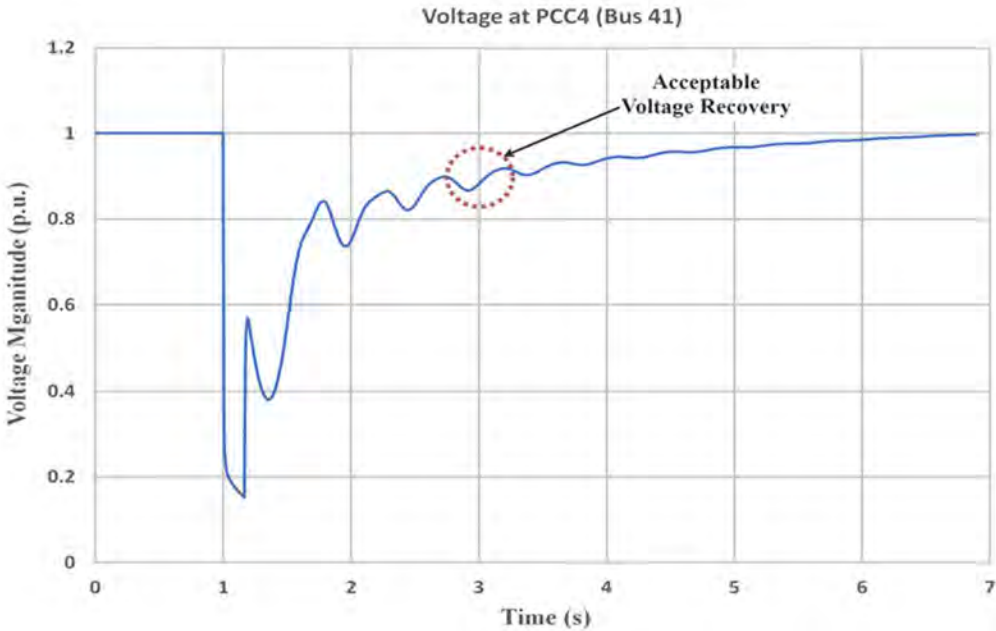


Figure 4.27: Voltage at PCC4 (Bus 41) at 30% RE penetration with SVC

The voltage magnitude after 2s of fault application is outlined in Table 4.5. It can be found that due to the proposed SVC placement algorithm, the post-fault voltages at all DER units stay above 0.88 p.u. Consequently, cascading tripping of DERs and subsequent blackout is prevented.

Table 4.5: Post-fault voltage with SVC after 2s of fault occurrence at 30% RE penetration

PCC	Voltage magnitude (p.u.)
PCC1(Bus 4)	0.9026
PCC2(Bus 100)	0.8813
PCC3(Bus 50)	0.8815
PCC4(Bus 41)	0.8819

### 4.5.3 Case-3: 40% RE Penetration

Similar to the previous cases, a three phase fault is applied at bus 31 through a reactance of  $j0.1 \Omega$  and is cleared after 10 cycles. The voltage at PCC1 (bus4) and PCC4 (bus 41) is shown in Figure 4.28 and 4.29 respectively. Similar voltage shapes are observed at other PCCs. The post-fault voltage magnitudes are summarized in Table 4.6.

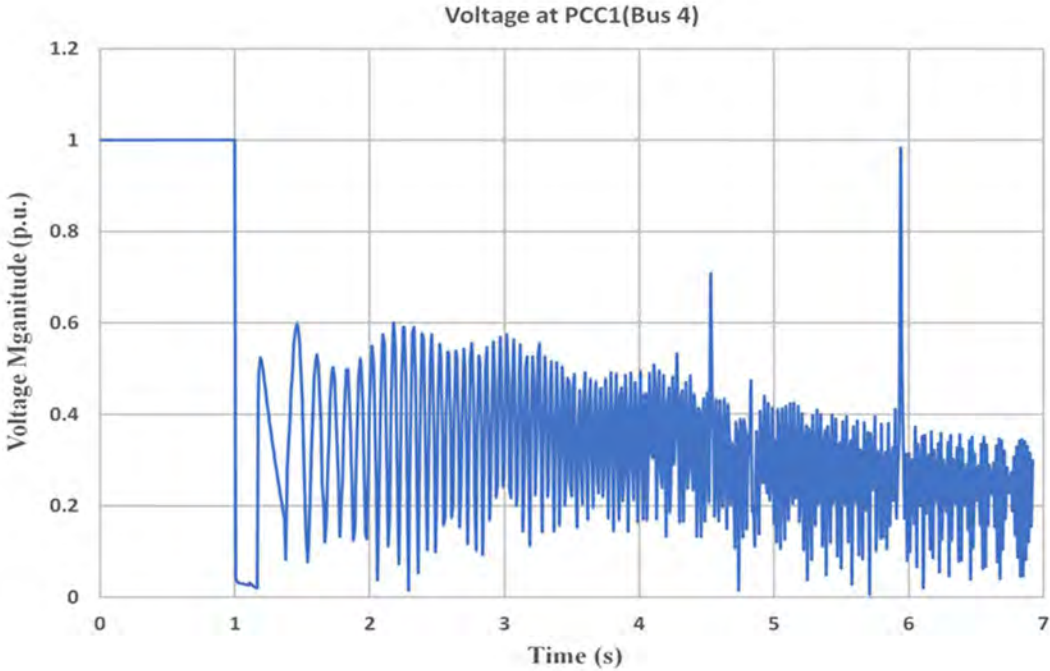


Figure 4.28: Voltage at PCC1 (Bus 4) at 40% RE penetration



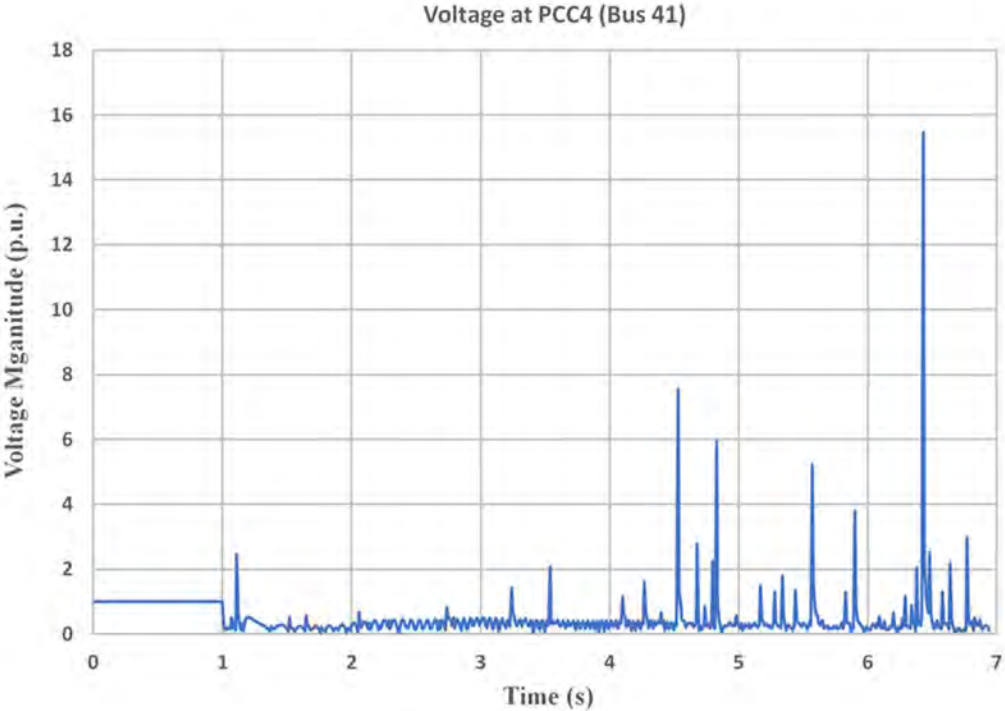


Figure 4.29: Voltage at PCC4 (Bus 41) at 40% RE penetration

Table 4.6: Post-fault voltage after 2s of fault occurrence at 40% RE penetration

PCC	Voltage magnitude (p.u.)
PCC1 (Bus 4)	0.263
PCC2 (Bus 100)	0.272
PCC3 (Bus 50)	0.367
PCC4 (Bus 41)	0.328

Since the PCC voltages fail to recover within stipulated time, all DER units sequentially trip. As a result, the microgrid faces a blackout.

In order to save the system at 40% RE penetration level, a SVC is connected at bus 21. The rating of this SVC is 2.6 MVAR, which is determined from the time domain simulations and the value of reactive power margin. With the placement of such centralized SVC, the post-fault voltage recovery performances of all DER units become satisfactory (i.e. more than 0.88 p.u.). Voltage recovery performance at PCC1 is shown in Figure 4.30 as an example.

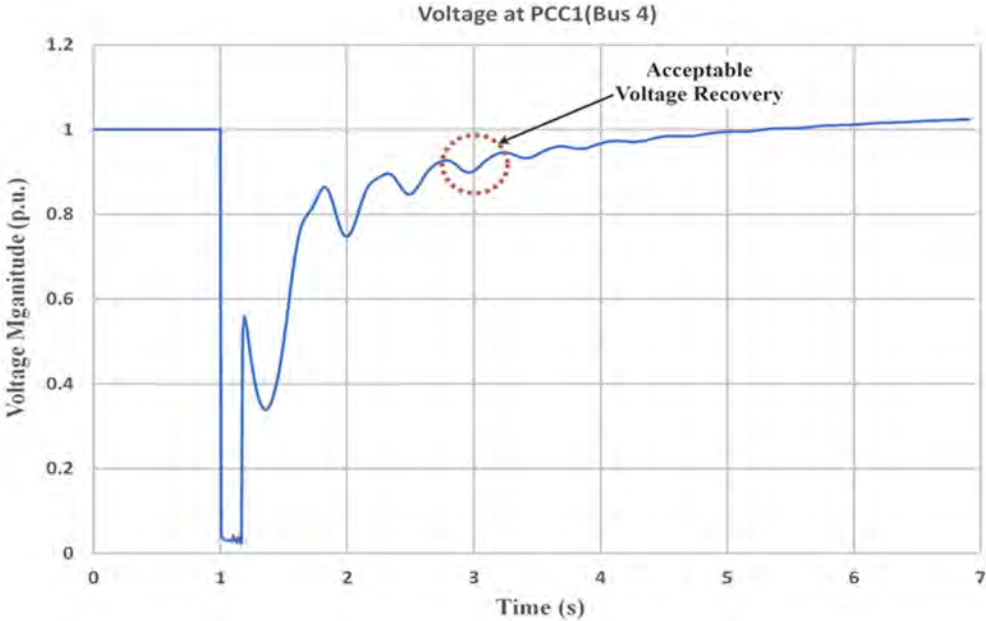


Figure 4.30: Voltage at PCC1 (Bus 4) at 40% RE penetration with SVC

Voltages at various PCCs after connecting SVC are summarized in Table 4.7. It can be found that with the proposed SVC placement algorithm, the post-fault voltages at all DER units become more than 0.88 p.u. Consequently, cascading tripping of DERs and resultant blackout is stopped.

Table 4.7: Post-fault voltage with SVC after 2s of fault occurrence at 40% RE penetration

PCC	Voltage magnitude (p.u.)
PCC1(Bus 4)	0.9012
PCC2(Bus 100)	0.8837
PCC3(Bus 50)	0.8844
PCC4(Bus 41)	0.8842

**4.5.4 Case-4: 45% RE Penetration**

In this scenario, nonrenewable diesel generators (DER1 and DER2) provide 10 MVA and 4.3 MVA respectively. In addition, the renewable sources (DER3 and DER4) supply 6 MVA and 5.7 MVA respectively. Like previous cases, time-domain simulations are carried out

for a three phase fault. Uncompensated voltage recovery performance at PCC1 is shown in Figure 4.31 as an example. Post-fault voltages at the all PCCs are summarized in Table 4.8.

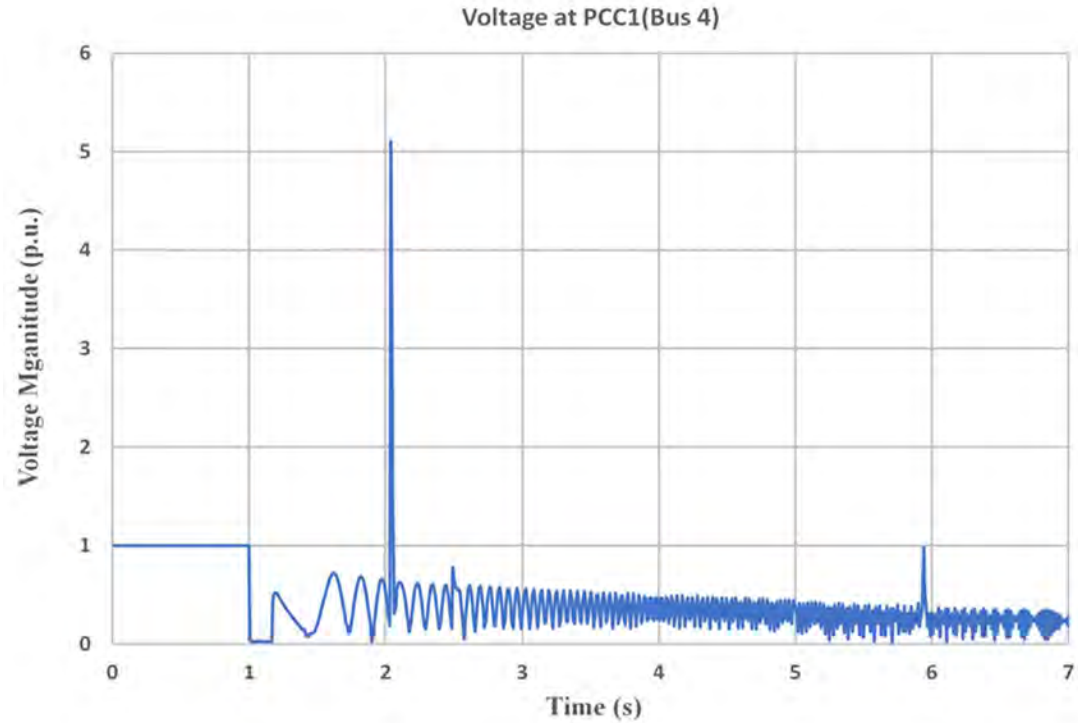


Figure 4.31: Voltage at PCC1 (Bus 4) at 45% RE penetration

Table 4.8: Post-fault voltage after 2s of fault occurrence at 45% RE penetration

PCC	Voltage magnitude (p.u.)
PCC1(Bus 4)	0.154
PCC2 (Bus 100)	0.112
PCC3 (Bus 50)	0.141
PCC4 (Bus 41)	0.059

It is found that the PCC voltages do not return to the acceptable limit within specified time. Therefore, all DER units consecutively trip and the microgrid encounters a blackout.

In order to avoid the blackout at 45% RE penetration level, a SVC is connected at bus 21 for compensation. The Q set point of this SVC is 2.88 MVAR. After connecting this centralized SVC, the post-fault voltage recovery performances of all DER units are found to be acceptable. Voltage recovery performance at PCC1 (i.e. bus 4) is shown in Figure 4.32 as an example.

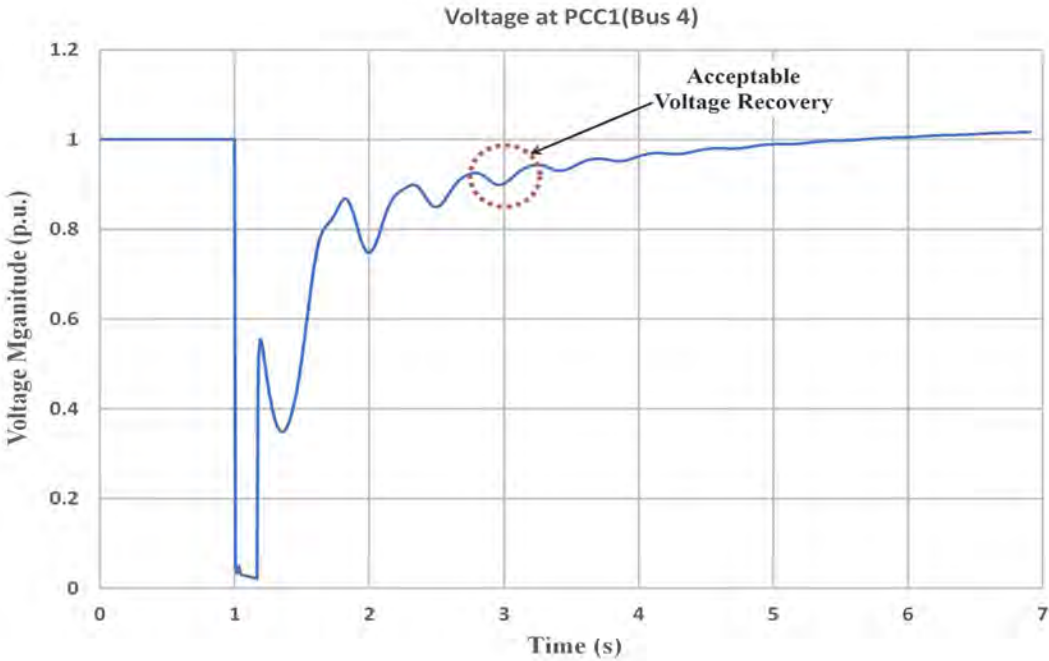


Figure 4.32: Voltage at PCC1 (Bus 4) at 45% RE penetration with SVC

Voltages at various PCCs after compensating with SVC are provided in Table 4.9. It can be revealed proposed SVC placement algorithm successfully retains the post-fault voltages of all DERs at the satisfactory level. Therefore, the system-wide blackout in the microgrid is stopped.

Table 4.9: Post-fault voltage with SVC after 2s of fault occurrence at 45% RE penetration

PCC	Voltage magnitude (p.u.)
PCC1(Bus 4)	0.9012
PCC2(Bus 100)	0.8883
PCC3(Bus 50)	0.8892
PCC4(Bus 41)	0.8893

**4.5.5 Case-5: 50% RE Penetration**

In this case, DER3 and DER4 collectively generate 13 MVA (out of 26 MVA total generation) to provide 50% renewable penetration level. Like previous cases, a three phase fault is applied at 1s through a reactance of  $j0.1 \Omega$  and cleared after 10 cycles. The voltage profile at PCC1 is shown in Figure 4.33 as an example. The post-fault voltage recovery characteristics of all PCCs are outlined in Table 4.10.

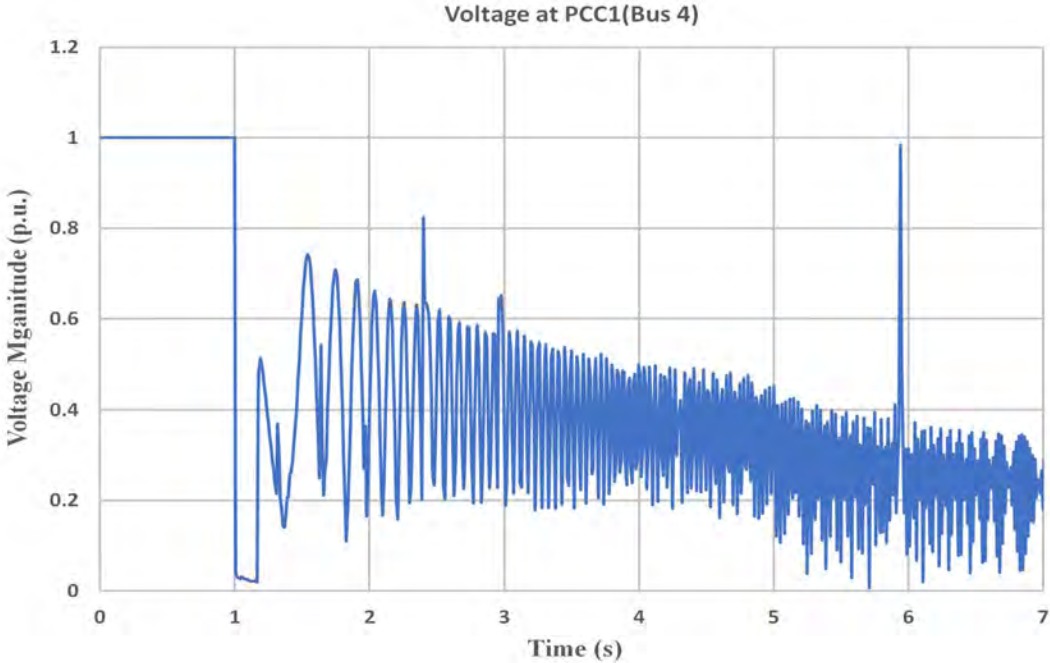


Figure 4.33: Voltage at PCC1 (Bus 4) at 50% RE penetration

Table 4.10: Post-fault voltage after 2s of fault occurrence at 50% RE penetration

PCC	Voltage magnitude (p.u.)
PCC1(Bus 4)	0.406
PCC2 (Bus 100)	0.368
PCC3 (Bus 50)	0.375
PCC4 (Bus 41)	0.372

It is observed that the PCC voltages are unable to come back to the tolerable limit within given time. Therefore, cascading tripping of DERs takes place and the microgrid experiences a blackout.

To stabilize the system voltage, a SVC is connected at bus 21 according to the developed algorithm. The rating of this SVC is found to be 2.9 MVAR. However, this SVC is not sufficient to bring the voltage at the PCCs over acceptable limit. Therefore, another SVC is connected at bus 37 (bus with next lowest reactive power margin) with a rating of 0.65 MVAR. Thus, in 50% RE penetration case, distributed placement approach of SVC is required. The voltage recovery performance at PCC1 is presented in Figure 4.34 as an example.

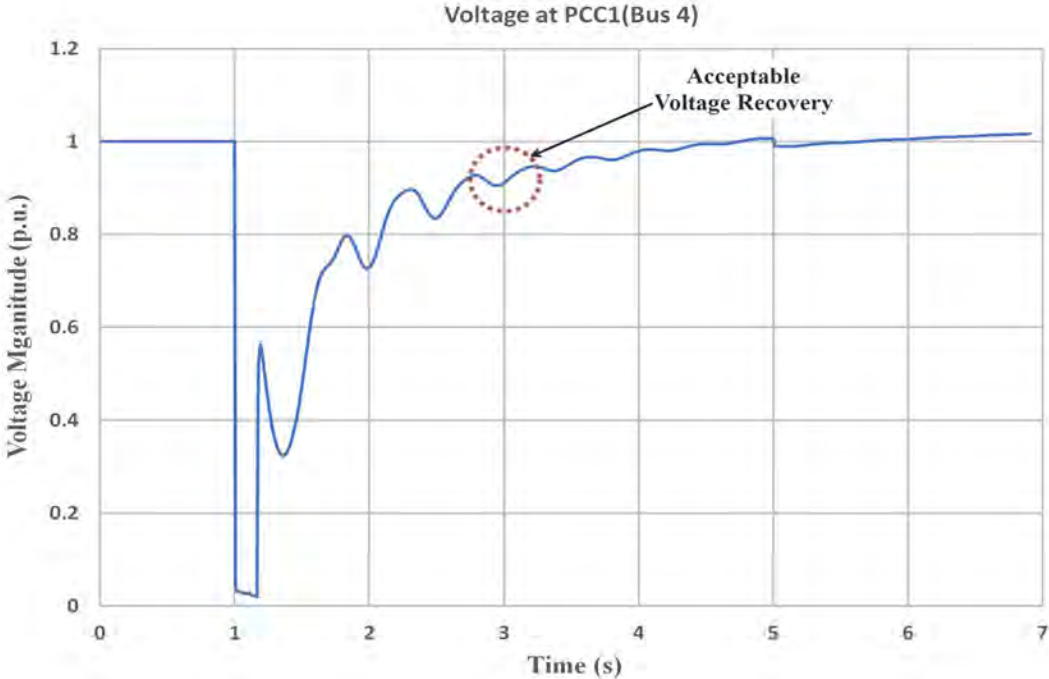


Figure 4.34: Voltage at PCC1 (Bus 4) at 50% RE penetration with SVC

Post-fault voltages at different PCCs after implementing the distributed SVC placement scheme are presented in Table 4.11. It can be noted that the proposed SVC placement method attains satisfactory post-fault voltage recovery for DER units. Hence, the cascading tripping of DERs and subsequent blackout in the microgrid are prevented.

Table 4.11: Post-fault voltage with SVCs after 2s of fault occurrence at 50% RE penetration

PCC	Voltage magnitude (p.u.)
PCC1(Bus 4)	0.9107
PCC2(Bus 100)	0.8806

PCC3(Bus 50)	0.8808
PCC4(Bus 41)	0.8800

### 4.6 Validation of the Proposed Methodology

To validate the proposed methodology, it is compared with a conventional (i.e. existing) SVC placement approach [53, 56-57]. In this approach, SVC is directly connected to the PCCs of DER units (unlike the proposed technique of connecting SVC based on reactive power margin). The post-fault voltage recovery performances under various RE penetration level using the existing approach are presented below.

**(i) 23% RE penetration level:** In 23% RE penetration level, it is found that a SVC with the rating of 2.07 MVAR provides satisfactory voltage recovery by deploying the proposed methodology. While existing technique is implemented, four SVCs are placed at four PCCs. The rating is each SVC is set to be 0.5175 MVAR. Therefore, the total SVC rating becomes 2.07 MVAR, which provides a rational basis for validation.

From time domain simulations, the post fault voltage magnitudes at different PCCs after 2s of fault application are recorded. Table 4.12 shows the results for the existing approach.

Table 4.12: Post-fault voltage with exiting approach at 23% RE penetration

PCC	Voltage magnitude after 2s of fault (p.u.)
PCC1(Bus 4)	0.8775
PCC2(Bus 100)	0.8660
PCC3(Bus 50)	0.8725
PCC4(Bus 41)	0.8961

It can be seen that only PCC4 recovers to the acceptable level (more than 0.88 p.u.), whereas the voltages at other PCCs fail to meet the grid requirement. However, in the proposed method, a SVC with the rating of 2.07 MVAR satisfactorily recovers all PCC voltages. Therefore, it is evident that the proposed methodology outperforms the conventional SVC placement approach.

**(ii) 30% RE penetration level:** In conventional approach, four SVCs each with a rating of 0.5875 MVAR are connected at four PCCs. From time domain simulations, the post fault voltage values at different PCCs after 2s of fault application are found. Table 4.13 shows the results for the conventional approach.

Table 4.13: Post-fault voltage with exiting approach at 30% RE penetration

PCC	Voltage magnitude after 2s of fault (p.u.)
PCC1(Bus 4)	0.8722
PCC2(Bus 100)	0.8630
PCC3(Bus 50)	0.8710
PCC4(Bus 41)	0.8940

When the conventional approach is followed three PCCs fail to attain satisfactory voltage recovery at 30% RE penetration. In contrast, all PCC voltages recover to acceptable level when the proposed algorithm is utilized.

**(iii) 40% RE penetration level:** In this scenario, four SVCs each with a rating of 0.65 MVAR are connected at four PCCs when the existing approach is taken into account. Table 4.14 shows the results of the post-fault voltages after 2s of fault application for the existing technique.

Table 4.14: Post-fault voltage with exiting approach at 40% RE penetration

PCC	Voltage magnitude after 2s of fault (p.u.)
PCC1(Bus 4)	0.8522
PCC2(Bus 100)	0.8375
PCC3(Bus 50)	0.8565
PCC4(Bus 41)	0.8677

It can be seen that none of the PCCs voltage recovers to satisfactory level while the existing method is implanted. On the contrary, the proposed methodology results in acceptable voltage recovery for all PCCs.



**(iv) 45% RE penetration level:** To implement the conventional approach, four SVCs each with a rating of 0.72 MVAR are connected at four PCCs. Table 4.15 contains the results of the post-fault voltages after 2s of fault application for the conventional method.

Table 4.15: Post-fault voltage with exiting approach at 45% RE penetration

PCC	Voltage magnitude after 2s of fault (p.u.)
PCC1(Bus 4)	0.8312
PCC2(Bus 100)	0.8261
PCC3(Bus 50)	0.8318
PCC4(Bus 41)	0.8555

It can be revealed that none of the PCCs voltage attains acceptable post-fault voltage recovery when the existing technique is applied. However, the proposed methodology provides satisfactory results in 45% RE penetration.

**(v) 50% RE penetration level:** In this case, four SVCs each with a rating of 0.8875 MVAR are connected at four PCCs when the existing approach is deployed. Table 4.16 outlines the magnitudes of the post-fault voltages after 2s of fault application for the existing approach.

Table 4.16: Post-fault voltage with exiting approach at 50% RE penetration

PCC	Voltage magnitude after 2s of fault (p.u.)
PCC1(Bus 4)	0.8055
PCC2(Bus 100)	0.7892
PCC3(Bus 50)	0.8012
PCC4(Bus 41)	0.8235

It can be noted that none of the PCCs voltage achieves satisfactory post-fault voltage recovery when the existing technique is utilized.

From the above simulations, it can be revealed that the existing SVC placement approach does not provide satisfactory post-fault voltage recovery in the microgrid. Conversely, the proposed algorithm gives acceptable voltage recovery to avoid DER tripping and resultant blackout. Therefore, the proposed methodology is more effective than the existing

approach. For ease of comparison, the performances of the both techniques are summarized in Table 4.17.

Table 4.17: Performance comparison under various RE penetration

RE penetration level (%)	SVC rating (MVAR)		Post-fault voltage recovery performance	
	Proposed approach	Existing approach	Proposed approach	Existing approach
23	2.07	2.07 (0.5175 x 4)	All PCCs satisfactorily recover	3 PCCs (out of 4) fail to satisfactorily recover
30	2.35	2.35 (0.5875 x 4)	All PCCs satisfactorily recover	3 PCCs (out of 4) fail to satisfactorily recover
40	2.60	2.60 (0.65 x 4)	All PCCs satisfactorily recover	All PCCs fail to satisfactorily recover
45	2.88	2.88 (0.72 x 4)	All PCCs satisfactorily recover	All PCCs fail to satisfactorily recover
50	3.55	3.55 (0.8875 x 4)	All PCCs satisfactorily recover	All PCCs fail to satisfactorily recover

## 4.7 Effect of Load Modeling

In this section, the impact of load models on the post-fault voltage recovery performance is comprehensively investigated using the proposed SVC placement approach. Simulation results presented in Section 4.6 are obtained for constant impedance load models. Therefore,

further simulations are carried out for constant current and constant power load models in this section.

#### 4.7.1 Constant Current Type Load Model

In this case, active and reactive power are modeled as constant current loads. SVCs are connected based on reactive power margin to provide satisfactory voltage recovery. In 23% RE penetration level, a centralized SVC with a rating of 2.30 MVAR is connected at bus 21. The post-fault voltages are provided in Table 4.18.

Table 4.18: Post-fault voltage for constant current load at 23% RE penetration

PCC	Voltage magnitude after 2s of fault (p.u.)
PCC1 (Bus 4)	0.9059
PCC2 (Bus 100)	0.8823
PCC3 (Bus 50)	0.8814
PCC4 (Bus 41)	0.8814

For other RE penetration level, the proposed algorithm is applied to the studied microgrid. The simulation results are given in Table 4.19. It can be noticed that at 45% and 50% RE penetration cases, distributed SVC placement approach is required when constant current load model is assumed. Also, the SVC rating increases with the increases of RE penetration level.

Table 4.19: Post-fault voltage for constant current load at 30%, 40%, 45% and 50% RE penetration

RE penetration level (%)	SVC location and rating	Voltage magnitude after 2s of fault (p.u.)			
		PCC1 (Bus 4)	PCC2 (Bus 100)	PCC3 (Bus 50)	PCC4 (Bus 41)
30	Bus 21, 2.52 MVAR	0.9045	0.8819	0.8815	0.8816
40	Bus 21, 2.83 MVAR	0.9068	0.8866	0.8866	0.8862

45	Bus 21, 2.90 MVAR Bus 37, 0.25 MVAR	0.8961	0.8806	0.8811	0.8808
50	Bus 21, 2.90 MVAR Bus 37, 0.95 MVAR	0.9188	0.8880	0.8875	0.8808

## 4.7.2 Constant Power Type Load Model

In this case, active and reactive power are modeled as constant power loads. Using the proposed algorithm, SVCs are placed based on reactive power margin to attain acceptable post-fault voltage recovery performance. Simulation results under various RE penetration cases are given in Table 4.20. It can be seen that until 40% RE penetration level, centralized SVC placement approach can provide satisfactory results. However, at 45% and 50% RE penetration cases, distributed SVC placement technique has to be deployed to avoid DER tripping and prevent blackout.

Table 4.20: Post-fault voltage for constant power load at different RE penetration

RE penetration level (%)	SVC location and rating	Voltage magnitude after 2s of fault (p.u.)			
		PCC1 (Bus 4)	PCC2 (Bus 100)	PCC3 (Bus 50)	PCC4 (Bus 41)
23	Bus 21, 2.60 MVAR	0.9141	0.8887	0.8869	0.8865
30	Bus 21, 2.72 MVAR	0.9082	0.8838	0.8823	0.8821
40	Bus 21, 2.90 MVAR	0.9034	0.8845	0.8835	0.8826
45	Bus 21, 2.90 MVAR Bus 37, 0.35 MVAR	0.9075	0.8937	0.8929	0.8829
50	Bus 21, 2.90 MVAR Bus 37, 1.0 MVAR	0.9708	0.9490	0.9478	0.9469

To compare the requirement of reactive compensation, Table 4.21 summarizes the total SVC ratings for different load models under various RE penetration cases.

Table 4.21: Comparison of SVC rating for different load models

RE penetration level (%)	SVC rating (MVAR)		
	Constant impedance load model	Constant current load model	Constant power load model
23	2.07	2.30	2.60

30	2.35	2.52	2.72
40	2.60	2.83	2.90
45	2.88	3.15	3.25
50	3.55	3.85	3.90

It can be revealed from the above table that at a specific RE penetration level, SVC rating (i.e. additional reactive power requirement) is the highest when constant power load model is considered. In contrast, constant impedance load model results in the lowest SVC requirement. For constant current load model, the SVC rating stays between that of constant impedance and constant power load models. Therefore, while applying the proposed methodology in a practical power system, the system operator needs to know the load behavior to determine the SVC rating. It will ensure satisfactory post-fault voltage recovery performance under all operating conditions.

## **CHAPTER 5**

### **Conclusions**

## 5.1 Conclusions

In this thesis, comprehensive investigations are carried out to mitigate the risk of blackout caused by inadequate post-fault voltage recovery performance at the PCCs of DER units in an islanded microgrid with high renewable penetration. As such, a methodology is developed to place SVC based on a voltage stability index called reactive power margin. The required SVC ratings to maintain satisfactory post-fault voltage recovery following a severe fault under various renewable penetration scenarios are evaluated. The proposed technique is validated by comparing its performance with that of an existing SVC placement approach. Furthermore, the impact of load modeling on the voltage recovery performance of DERs is explored. To this end, constant impedance, constant current and constant power type of load models are taken into account. The key findings of this research work are summarized as follows.

- i. A microgrid operating in an islanded mode is prone to unacceptable post-fault voltage recovery performance at the PCCs of DERs, which can lead to tripping of DER units. Consecutive tripping of DER units can eventually cause the blackout of the whole system.
- ii. The higher renewable power penetration makes it more challenging to attain adequate post-fault voltage recovery performance to avert the possibility of blackout.
- iii. Connecting SVC units with appropriate rating at the weakest buses can bring the post-fault voltage at the PCCs above the acceptable limit within specified time. Therefore, tripping of DER units can be avoided following a severe fault.
- iv. The required SVC rating for retaining satisfactory post-fault voltage recovery enactment shows increasing trend when the renewable penetration level increases.
- v. Placing multiple SVCs directly at the PCCs of DERs (by keeping the total SVC rating unchanged obtained from the proposed methodology) does not provide satisfactory post-fault voltage recovery. Thus, the risk of blackout still exists while the conventional SVC placement method is utilized. It eventually indicates that the proposed technique is more effective than the conventional one to avoid DER tripping and subsequent blackout in an islanded microgrid in presence of high renewable generation.
- vi. In a particular renewable penetration level, SVC rating becomes the highest when active and reactive power are modeled as constant power load. On the contrary, constant impedance load model provides the lowest value of additional reactive power requirement. Furthermore, the SVC rating stays between that of constant impedance

and constant power load models when the constant current load model is used. Therefore, a proper load model is an important aspect for finding the SVC rating in a microgrid.

## 5.2 Future Research Scopes

The following scopes can be suggested as the extension of the present research work for further improvement.

- i. In this work, SVC is deployed to improve the post-fault voltage recovery performance in an islanded microgrid. As such, the possibility of utilizing another FACTS device, STATCOM, can be explored.
- ii. Reactive power margin is used as a voltage stability index in this work to identify the weakest bus for placing reactive power compensation device. Similarly, other voltage stability indices viz. Fast Voltage Stability Index (FVSI) and Voltage Sensitivity Factor (VSF) can be employed.
- iii. Simulation results indicate that the system voltage wave shapes have oscillatory patterns after fault occurrence when no reactive compensation is done in higher renewable penetration cases. This may be due to small signal oscillation, which needs further investigations.
- iv. The impact of composite load models (i.e. a combination of constant impedance, constant current and constant power) on the post-fault voltage recovery can be explored.
- v. The appropriate size of reactive support devices can be estimated using optimization techniques.

## Bibliography

- [1] IEA, "Energy related CO<sub>2</sub> emissions, 1990-2019", IEA, Paris <https://www.iea.org/data-and-statistics/charts/energy-related-co2-emissions-1990-2019>
- [2] <https://www.thedailystar.net/bangladesh-blackout-2014-48574>

- [3] Kyriacou, A., Demetriou, P., Panayiotou, C. and Kyriakides, E., “Controlled Islanding Solution for Large-Scale Power Systems”, *IEEE Transactions on Power Systems*, vol. 33, no. 2, pp. 1591-1602, 2018.
- [4] Akorede, M. F., Hizam, H., & Pouresmaeil, E., “Distributed energy resources and benefits to the environment. *Renewable and sustainable energy reviews*”, 14(2), 724-734. (2010)
- [5] Coster, E. J., Myrzik, J. M., Kruimer, B., & Kling, W. L., “Integration issues of distributed generation in distribution grids. *Proceedings of the IEEE*”, 99(1), 28-39, 2010.
- [6] Lasseter, R. H. *Microgrids and distributed generation. Journal of Energy Engineering*, 133(3), 144-149, 2007.
- [7] Marnay, C., & Venkataramanan, G., “Microgrids in the evolving electricity generation and delivery infrastructure”, In 2006 IEEE power engineering society general meeting (pp. 5-pp). IEEE. (2006, June)
- [8] Meegahapola, L. G., Robinson, D., Agalgaonkar, A. P., Perera, S., & Ciufu, P., “Microgrids of commercial buildings: Strategies to manage mode transfer from grid connected to islanded mode”, *IEEE Transactions on sustainable energy*, 5(4), 1337-1347, 2014.
- [9] Barnes, M., Kondoh, J., Asano, H., Oyarzabal, J., Ventakaramanan, G., Lasseter, R., & Green, T., “Real-world microgrids-an overview”, In 2007 IEEE International Conference on System of Systems Engineering (pp. 1-8). IEEE, April, 2007.
- [10] de Souza, A. Z., Portelinha, F. M., Marujo, D., & Oliveira, D. Q., “Microgrids Operation in Islanded Mode”, In *Sustainable Development in Energy Systems* (pp. 193-215). Springer, Cham, 2017.
- [11] Su, W., & Wang, J., “Energy management systems in microgrid operations”, *The Electricity Journal*, 25(8), 45-60, 2012.
- [12] Parhizi, S., Lotfi, H., Khodaei, A., & Bahramirad, S., “State of the art in research on microgrids: A review”, *Ieee Access*, 3, 890-925, 2015.
- [13] Kaur, A., Kaushal, J., & Basak, P., “A review on microgrid central controller”, *Renewable and Sustainable Energy Reviews*, 55, 338-345, 2016.
- [14] Lopes, J. P., Moreira, C. L., & Madureira, A. G., “Defining control strategies for microgrids islanded operation”, *IEEE Transactions on power systems*, 21(2), 916-924, 2006.



- [15] Crucitti, P., Latora, V., & Marchiori, M., “Model for cascading failures in complex networks”, *Physical Review E*, 69(4), 045104, 2004.
- [16] Chakraborty, N. C., Banerji, A., & Biswas, S. K., “Survey on major blackouts analysis and prevention methodologies”, 2015.
- [17] Papazoglou, T. M., & Gigandidou, A., “Impact and benefits of distributed wind generation on quality and security in the case of the Cretan EPS”, In *CIGRE/IEEE PES International Symposium Quality and Security of Electric Power Delivery Systems*, 2003. CIGRE/PES 2003. (pp. 193-197). IEEE, October, 2003.
- [18] Union of the Co-ordination of Transmission of Electricity - UCTE, “Final report - System Disturbance on 4 November 2006”, 2007.
- [19] Edris, A. A., “Proposed terms and definitions for flexible AC transmission system (FACTS)”, *IEEE Transactions on Power Delivery*, 12(4), 1997.
- [20] Dehkordi, N. M., Sadati, N., & Hamzeh, M. A., “Backstepping high-order sliding mode voltage control strategy for an islanded microgrid with harmonic/interharmonic loads”, *Control Engineering Practice*, 58, 150-160, 2017.
- [21] Hirase, Y., Abe, K., Sugimoto, K., Sakimoto, K., Bevrani, H., & Ise, T. A., “Novel control approach for virtual synchronous generators to suppress frequency and voltage fluctuations in microgrids”, *Applied Energy*, 210, 699-710, 2018.
- [22] Siddique, A. B., Munsif, M. S., Sarker, S. K., Das, S. K., & Islam, M. R., “Voltage and current control augmentation of islanded microgrid using multifunction model reference modified adaptive PID controller”, *International Journal of Electrical Power & Energy Systems*, 113, 492-501, 2019.
- [23] Kim, J. Y., Park, J. H., & Lee, H. J., “Coordinated control strategy for microgrid in grid-connected and islanded operation”, *IFAC Proceedings Volumes*, 44(1), 14766-14771, 2011.
- [24] Garmabdari, R., Moghimi, M., Yang, F., Gray, E., & Lu, J., “Multi-objective energy storage capacity optimisation considering Microgrid generation uncertainties”, *International Journal of Electrical Power & Energy Systems*, 119, 105908, 2020.
- [25] Acharya, S., El Moursi, M. S., & Al-Hinai, A., “Coordinated frequency control strategy for an islanded microgrid with demand side management capability”, *IEEE Transactions on Energy Conversion*, 33(2), 639-651, 2017.

- [26] Serban, I., & Marinescu, C., “Battery energy storage system for frequency support in microgrids and with enhanced control features for uninterruptible supply of local loads”, *International Journal of Electrical Power & Energy Systems*, 54, 432-441, 2014.
- [27] Aghamohammadi, M. R., & Abdolahinia, H., “A new approach for optimal sizing of battery energy storage system for primary frequency control of islanded microgrid”, *International Journal of Electrical Power & Energy Systems*, 54, 325-333, 2014.
- [28] García-Plaza, M., Carrasco, J. E. G., Alonso-Martínez, J., & Asensio, A. P., “Peak shaving algorithm with dynamic minimum voltage tracking for battery storage systems in microgrid applications”, *Journal of Energy Storage*, 20, 41-48, 2018.
- [29] Fortenbacher, P., Ulbig, A., & Andersson, G., “Optimal placement and sizing of distributed battery storage in low voltage grids using receding horizon control strategies”, *IEEE Transactions on Power Systems*, 33(3), 2383-2394, 2017.
- [30] Palizban, O., & Kauhaniemi, K., “Distributed cooperative control of battery energy storage system in AC microgrid applications”, *Journal of Energy Storage*, 3, 43-51, 2015.
- [31] Thrampoulidis, C., Bose, S., & Hassibi, B., “Optimal placement of distributed energy storage in power networks”, *IEEE Transactions on Automatic Control*, 61(2), 416-429, 2015.
- [32] El-Bidairi, K. S., Nguyen, H. D., Mahmoud, T. S., Jayasinghe, S. D. G., & Guerrero, J. M., “Optimal sizing of Battery Energy Storage Systems for dynamic frequency control in an islanded microgrid: A case study of Flinders Island, Australia”, *Energy*, 195, 117059, 2020.
- [33] Kerdphol, T., Fuji, K., Mitani, Y., Watanabe, M., & Qudaih, Y., “Optimization of a battery energy storage system using particle swarm optimization for stand-alone microgrids”, *International Journal of Electrical Power & Energy Systems*, 81, 32-39, 2016.
- [34] Kerdphol, T., Qudaih, Y., & Mitani, Y., “Optimum battery energy storage system using PSO considering dynamic demand response for microgrids”, *International Journal of Electrical Power & Energy Systems*, 83, 58-66, 2016.
- [35] Hesaroor, K., & Das, D., “Optimal sizing of energy storage system in islanded microgrid using incremental cost approach”, *Journal of Energy Storage*, 24, 100768, 2019.

- [36] Yamchi, H. B., Shahsavari, H., Kalantari, N. T., Safari, A., & Farrokhifar, M., “A cost-efficient application of different battery energy storage technologies in microgrids considering load uncertainty”, *Journal of Energy Storage*, 22, 17-26, 2019.
- [37] Jia, H., Mu, Y., & Qi, Y., “A statistical model to determine the capacity of battery–supercapacitor hybrid energy storage system in autonomous microgrid”, *International Journal of Electrical Power & Energy Systems*, 54, 516-524, 2014.
- [38] Arani, A. K., Karami, H., Gharehpetian, G. B., & Hejazi, M. S. A., “Review of Flywheel Energy Storage Systems structures and applications in power systems and microgrids”, *Renewable and Sustainable Energy Reviews*, 69, 9-18, 2017.
- [39] Yang, L., Tai, N., Fan, C., & Meng, Y., “Energy regulating and fluctuation stabilizing by air source heat pump and battery energy storage system in microgrid”, *Renewable energy*, 95, 202-212, 2016.
- [40] Pilloni, A., Pisano, A., & Usai, E., “Voltage restoration of islanded microgrids via cooperative second-order sliding mode control”, *IFAC-PapersOnLine*, 50(1), 9637-9642, 2017.
- [41] Soto, D., Edrington, C., Balathandayuthapani, S., & Ryster, S., “Voltage balancing of islanded microgrids using a time-domain technique”, *Electric power systems research*, 84(1), 214-223, 2012.
- [42] Aziz, T., Masood, N. A., Deeba, S. R., Tushar, W., & Yuen, C., “A methodology to prevent cascading contingencies using BESS in a renewable integrated microgrid”, *International Journal of Electrical Power & Energy Systems*, 110, 737-746, 2019.
- [43] Karavas, C. S., Kyriakarakos, G., Arvanitis, K. G., & Papadakis, G., “A multi-agent decentralized energy management system based on distributed intelligence for the design and control of autonomous polygeneration microgrids”, *Energy Conversion and Management*, 103, 166-179, 2015.
- [44] Kyriakarakos, G., Dounis, A. I., Arvanitis, K. G., & Papadakis, G., “A fuzzy cognitive maps–petri nets energy management system for autonomous polygeneration microgrids”, *Applied Soft Computing*, 12(12), 3785-3797, 2012.
- [45] Schoonenberg, W. C., & Farid, A. M., “A dynamic model for the energy management of microgrid-enabled production systems”, *Journal of cleaner production*, 164, 816-830, 2017.

- [46] Anvari-Moghaddam, A., Rahimi-Kian, A., Mirian, M. S., & Guerrero, J. M., “A multi-agent based energy management solution for integrated buildings and microgrid system”, *Applied energy*, 203, 41-56, 2017.
- [47] Meng, L., Sanseverino, E. R., Luna, A., Dragicevic, T., Vasquez, J. C., & Guerrero, J. M., “Microgrid supervisory controllers and energy management systems: A literature review”, *Renewable and Sustainable Energy Reviews*, 60, 1263-1273, 2016.
- [48] Chettibi, N., & Mellit, A., “Intelligent control strategy for a grid connected PV/SOFC/BESS energy generation system”, *Energy*, 147, 239-262, 2018.
- [49] Sedighizadeh, M., Esmaili, M., Jamshidi, A., & Ghaderi, M. H., “Stochastic multi-objective economic-environmental energy and reserve scheduling of microgrids considering battery energy storage system”, *International Journal of Electrical Power & Energy Systems*, 106, 1-16, 2019.
- [50] Koochi-Kamali, S., & Rahim, N. A., “Coordinated control of smart microgrid during and after islanding operation to prevent under frequency load shedding using energy storage system”, *Energy conversion and management*, 127, 623-646, 2016.
- [51] Nasr, M. A., Nikkhah, S., Gharehpetian, G. B., Nasr-Azadani, E., & Hosseinian, S. H., “A multi-objective voltage stability constrained energy management system for isolated microgrids”, *International Journal of Electrical Power & Energy Systems*, 117, 105646, 2020.
- [52] Wang, J., Zhao, C., Pratt, A., & Baggu, M., “Design of an advanced energy management system for microgrid control using a state machine”, *Applied energy*, 228, 2407-2421, 2018.
- [53] Kincic, S., Wan, X. T., McGillis, D. T., Chandra, A., Ooi, B. T., Galiana, F. D., & Joos, G., “Voltage support by distributed static VAR systems (SVS)”, *IEEE transactions on power delivery*, 20(2), 1541-1549, 2005.
- [54] Chen, J. H., Lee, W. J., & Chen, M. S., “Using a static var compensator to balance a distribution system”, In *IAS'96. Conference Record of the 1996 IEEE Industry Applications Conference Thirty-First IAS Annual Meeting (Vol. 4, pp. 2321-2326)*, IEEE, 1996.
- [55] Cathey, J. J., & Moore, W. E., “Improvement of generator output and stability margin by use of a dedicated static VAR compensator”, *Electric Power Systems Research*, 63(2), 119-125, 2002.

- [56] Gabbar, H. A., & Abdelsalam, A. A., “Microgrid energy management in grid-connected and islanding modes based on SVC”, *Energy Conversion and Management*, 86, 964-972, 2014.
- [57] Mohanty, A., Viswavandya, M., Mohanty, S., & Mishra, D. K., “Intelligent Controller based SVC for voltage stability improvement in a Stand-alone wind-diesel-micro hydro hybrid system”, *Procedia Computer Science*, 57, 1308-1316, 2015.
- [58] Viswavandya, M., Mohanty, A., Ray, P. K., & Paramita, P., “Restoration of stable voltage in an isolated hybrid solar power system with combined JAYA-DE algorithm”, *Optik*, 180, 536-548, 2019.
- [59] Renmu, H., Jin, M., & Hill, D. J., “Composite load modeling via measurement approach”, *IEEE Transactions on power systems*, 21(2), 663-672, 2006.
- [60] Arif, A., Wang, Z., Wang, J., Mather, B., Bashualdo, H., & Zhao, D., “Load modeling—A review”, *IEEE Transactions on Smart Grid*, 9(6), 5986-5999, 2017.
- [61] Mota, L. T. M., & Mota, A. A., “Load modeling at electric power distribution substations using dynamic load parameters estimation”, *International Journal of Electrical Power & Energy Systems*, 26(10), 805-811, 2004.
- [62] Zhao, J., Wang, Z., & Wang, J., “Robust time-varying load modeling for conservation voltage reduction assessment”, *IEEE Transactions on Smart Grid*, 9(4), 3304-3312, 2016.
- [63] Vaahedi, E., El-Din, H. Z., & Price, W. W., “Dynamic load modeling in large scale stability studies”, *IEEE Transactions on Power Systems*, 3(3), 1039-1045, 1988.
- [64] El-Shimy, M., Mostafa, N., Afandi, A. N., Sharaf, A. M., & Attia, M. A., “Impact of load models on the static and dynamic performances of grid-connected wind power plants: A comparative analysis”, *Mathematics and Computers in Simulation*, 149, 91-108, 2018.
- [65] Singh, B., Mukherjee, V., & Tiwari, P., “Genetic algorithm optimized impact assessment of optimally placed DGs and FACTS controller with different load models from minimum total real power loss viewpoint”, *Energy and Buildings*, 126, 194-219, 2016.
- [66] Hashemi-Dezaki, H., Hariri, A. M., & Hejazi, M. A., “Impacts of load modeling on generalized analytical reliability assessment of smart grid under various penetration levels of wind/solar/non-renewable distributed generations”, *Sustainable Energy, Grids and Networks*, 20, 100246, 2019.

- [67] IEEE Standards Association, “IEEE Standard for Interconnection and Interoperability of Distributed Energy Resources with Associated Electric Power Systems Interfaces – IEEE Std 1547-2018”, pp.1-138, 2018.
- [68] Kundur, P., Balu, N. J., & Lauby, M. G., “Power system stability and control (Vol. 7)”, New York: McGraw-hill, 1994.
- [69] Milanović, J. V., “On unreliability of exponential load models. Electric power systems research”, 49(1), 1-9, 1999.
- [70] DIgSILENT GmbH, DIgSILENT PowerFactory V15.1-User Manual, 2013.
- [71] IEEE Recommended Practice for Industrial and Commercial Power Systems Analysis, IEEE Std 399-1997, 1998.